INFRARED SIGNATURES OF DISRUPTED MINOR PLANETS AT WHITE DWARFS

J. Farihi[1,2,3], M. Jura[2], and B. Zuckerman[2]

ABSTRACT

Spitzer Space Observatory IRAC and MIPS photometric observations are presented for 20 white dwarfs with $T_{\rm eff} \lesssim 20,000$ K and metal-contaminated photospheres. A warm circumstellar disk is detected at GD 16 and likely at PG 1457−086, while the remaining targets fail to reveal mid-infrared excess typical of dust disks, including a number of heavily polluted stars. Extending previous studies, over 50% of all single white dwarfs with implied metal accretion rates $dM/dt \gtrsim 3 \times 10^8$ g s^{-1} display a warm infrared excess from orbiting dust; the likely result of a tidally-destroyed minor planet. This benchmark accretion rate lies between the dust production rates of 10^6 g s^{-1} in the solar system zodiacal cloud and 10^{10} g s^{-1} often inferred for debris disks at main sequence A-type stars. It is estimated that between 1% and 3% of all single white dwarfs with cooling ages less than around 0.5 Gyr possess circumstellar dust, signifying an underlying population of minor planets.

Subject headings: circumstellar matter— infrared: stars– minor planets, asteroids— planetary systems – stars: abundances— stars: evolution— stars: individual (GD 16, PG 1457−086)— stars: low-mass, brown dwarfs — white dwarfs

1. INTRODUCTION

Known extrasolar planetary systems orbiting main sequence stars consist of a few large planets such as Jupiter (Cumming et al. 2008), and/or, as demonstrated by studies of debris disks, numerous minor planets analogous to solar system asteroids and Kuiper belt objects

[1]Department of Physics & Astronomy, University of Leicester, University Road, Leicester LE1 7RH, UK; jf123@star.le.ac.uk

[2]Department of Physics & Astronomy, University of California, 430 Portola Plaza, Los Angeles, CA 90095; jura,ben@astro.ucla.edu

[3]Gemini Observatory, Northern Operations, 670 North A'ohoku Place, Hilo, HI 96720

(Zuckerman 2001). Apparently, the assembly of planets from planetesimals is inefficient, and stars possess complex populations of orbiting material (see Ida & Lin 2008 and references therein).

Relative to main sequence stars, white dwarfs offer two advantages for the study of extrasolar planetary systems. First, white dwarfs are earth-sized and their low luminosities permit the direct detection of infrared emission from cool self-luminous companions such as brown dwarfs and massive jovian planets (Farihi et al. 2008a; Burleigh et al. 2006; Farihi et al. 2005a; Zuckerman & Becklin 1987a; Probst 1983). Second, cool white dwarfs should be atmospherically free of heavy elements (Zuckerman et al. 2003; Alcock et al. 1986; Paquette et al. 1986), and those stars with planetary system remnants can become spectroscopically contaminated by small, but detectable, amounts of accreted material. Analysis of metal-polluted white dwarfs enables an indirect, yet detailed and powerful compositional analysis of extrasolar planetary matter; Zuckerman et al. (2007) found that the abundances in the spectacularly metal-rich white dwarf GD 362 are consistent with the accretion of a large asteroid with composition similar to the Earth-Moon system.

The most metal-contaminated white dwarfs often display evidence of circumstellar disks; either by infrared excess (Farihi et al. 2008b; Kilic & Redfield 2007; von Hippel et al. 2007; Jura et al. 2007a; Kilic et al. 2006; Becklin et al. 2005; Kilic et al. 2005; Graham et al. 1990; Zuckerman & Becklin 1987b), or by broad, double-peaked optical emission lines (Gänsicke et al. 2008, 2007, 2006), or both (Melis et al. 2008; Brinkworth et al. 2008). Evidence is strong that these disks evolve from the tidal disruption of minor planets (Jura 2008, 2003). To be tidally destroyed within the Roche limit of a white dwarf, an asteroid needs to be perturbed from its orbit, and hence unseen planets of conventional size are expected at white dwarfs with dusty disks.

Including the disks around GD 16 and PG 1457−086, which are reported in this paper, the number of white dwarfs with circumstellar disks is 14 (see Table 1). Although at least half a dozen publications present *Spitzer* observations of white dwarfs, there has not yet been a thorough search of metal-rich white dwarfs for cool dust at longer, MIPS wavelengths, nor a focus on those contaminated degenerates with helium-rich atmospheres; this study bridges that gap and analyzes all 53 metal-rich degenerates observed by *Spitzer*. The numbers are now large enough that one can investigate the presence of a disk as a function of cooling age and metal accretion rate.

This paper presents the results of an IRAC $3 - 8$ μm and MIPS 24 μm photometric search for mid-infrared excess due to circumstellar dust at cool, metal-contaminated white dwarfs. The goals of the study are: 1) to constrain the frequency of dust disks around white dwarfs as a function of cooling age; and 2) to combine all available *Spitzer* data on metal-rich

white dwarfs to better understand their heavy element pollutions.

2. OBSERVATIONS AND DATA

Metal-rich white dwarf targets were imaged over $3 - 8$ μm with the InfraRed Array Camera (IRAC, $1.20''$ pixel^{-1}; Fazio et al. 2004) using all four bandpasses, and at 24 μm with the Multiband Imaging Photometer for *Spitzer* (MIPS, $2.45''$ pixel^{-1} ; Rieke et al. 2004). Observations analyzed here are primarily taken from *Spitzer* Cycle 3 Program 30387 and those previously published in Jura et al. (2007a), with several archival datasets also included. Twenty newly observed or analyzed white dwarf targets are listed in Table 2, representing near equal numbers of DAZ and DBZ stars, and including G180-57 and HS 2253+803, two examples of metal-rich yet carbon-deficient stars. Several Table 2 stars have been previously imaged with IRAC in other programs, hence for those stars only the MIPS observations are unique to this work; their IRAC data were extracted from the *Spitzer* archive and analyzed independently here. For two metal-rich white dwarf targets of particular interest, vMa 2 and LTT 8452, both IRAC and MIPS data were extracted from the *Spitzer* archive. The primary datasets utilized IRAC individual frame times of 30 s in a 20-point, medium-scale dither pattern, for a total exposure time of 600 s in each of the four filters at each star. MIPS 24 μm observations were executed using 10 s individual frame times with the default 14-point dither pattern, repeated for 10 cycles, yielding a 1400 s total exposure time for each science target. Table 3 lists the IRAC and MIPS fluxes with errors and upper limits for all Table 2 white dwarfs, and also the non-metal-rich white dwarfs NLTT 3915 and LHS 46; these two stars are discussed in §3.6.

Data reduction and photometry, including 3σ upper limits for non-detections, were performed as described in Farihi et al. (2008a,b), and Jura et al. (2007a,b), but photometric errors were not treated as conservatively. To account for the faintest MIPS 24 μm detections, and for reasons of consistency, the photometric measurement errors for both IRAC and MIPS were taken to be the Gaussian noise in an $r = 2$ pixel aperture at all wavelengths; i.e. the sky noise per pixel multiplied by the square root of the aperture area. IRAC data at 3.6 and 4.5 μm are typically high signal-to-noise (S/N $\gtrsim$ 50) and therefore dominated by a 5% calibration uncertainty (Farihi et al. 2008b; Jura et al. 2007a), whereas data at 5.7 and 7.9 μm have total errors which are a combination of calibration and photometric measurement errors. Most of the MIPS 24 μm detections are dominated by the photometric measurement errors, with a 10% calibration uncertainty employed for these data (Engelbracht et al. 2007). In actuality, the photometric errors may be somewhat larger for reasons described in detail elsewhere; namely crowded fields for the two short wavelength IRAC channels, and

non-uniform sky backgrounds for the two longer wavelength IRAC channels and for MIPS (Farihi et al. 2008b). Among the 20 science targets imaged at 24 μm and analyzed here, the background noise varied significantly, as evidenced by the variance among the 1σ errors and 3σ upper limits in Table 3 (and similar variance among the 24 μm data in Table 1 of Jura et al. 2007a).

3. ANALYSIS AND RESULTS

Figures 1−8 plot the spectral energy distributions (SEDs) of the 20 metal-rich stars listed in Table 2, grouped by right ascension, including *Spitzer* photometry and upper limits. Optical and near-infrared photometric data were taken from: Table 2 references; McCook & Sion (2006) and references therein, Salim & Gould (2003), Monet et al. (2003), and the 2MASS point source catalog (Skrutskie et al. 2006). The data were fitted with blackbodies of the appropriate temperature (i.e. able to reproduce the photospheric flux), which are sufficient to recognize excess emission at the 3σ level. Of all the targets, only GD 16 and PG 1457−086 display photometric excess above this threshold in their IRAC or MIPS observations.

3.1. GD 16

Figure 2 displays the *Spitzer* photometry for GD 16, which reveals a prominent mid-infrared excess indicative of $T \sim 1000$ K circumstellar dust. The 2MASS data on this star appear to indicate an infrared excess at H and K bands, but it is likely these data are unreliable; independent near-infrared photometry at high S/N (Farihi et al. 2009, in preparation) indicate an excess only at K-band, as seen in Figure 2. No published optical photoelectric photometry exists, but photographic data indicate $V \approx 15.5$ mag from both USBO-B1 and the original discovery paper (Monet et al. 2003; Giclas et al. 1965); this V-band flux is plotted and agrees well with the measured near-infrared fluxes for a white dwarf of the appropriate temperature.

A detailed optical spectral analysis of GD 16 by Koester et al. (2005b) yielded atmospheric parameters $T_{\rm eff} = 11,500$ K, [H/He] $= -2.9$, and $M_V = 12.05$ mag, with the assumption of $\log g = 8.0$. Using the measured $J = 15.55$ mag together with the model-predicted $V - J = 0.09$ color for the relevant effective temperature, surface gravity, and helium-rich composition, the white dwarf is expected to have $M_J = 12.14$ mag and hence a nominal photometric distance of $d = 48$ pc (Bergeron et al. 1995a,b). Figure 9 shows a fit to the

thermal dust emission using the flat ring model of Jura (2003). This model does an excellent job of reproducing all infrared data from 2.2 μm onwards. For an 11,500 K star, the Figure 9 inner and outer dust temperatures correspond to 12 and 30 stellar radii, or 0.15 and 0.39 $R_{\odot}$ respectively (Chiang & Goldreich 1997). The fractional disk luminosity, $\tau = L_{\mathrm{IR}}/L = 0.02$, is about 2/3 that of the disks at G29-38, GD 362, and GD 56 (Farihi et al. 2008b; Jura et al. 2007a).

3.2. PG 1457−086

Spitzer photometry for PG 1457−086 is shown in Figure 5, and reveals flux excess just over 3σ at both 3.6 and 4.5 μm, relative to the expected photospheric flux. The 2MASS photometry for this white dwarf at H and K bands has large errors, and independent near-infrared photometry at high S/N (Farihi et al. 2009, in preparation) indicate a probable, slight excess at K band. Overall, the infrared excess is mild but indicative of very warm, $T \sim 1500$ K emission. Koester et al. (2005a) and Liebert et al. (2005) derive $T_{\mathrm{eff}} = 20,400$ K and 21,500 K, respectively for PG 1457−086, while both find a surface gravity log $g \approx 8.0$. The 20,400 K value was employed for the figures because it is more conservative, predicting slightly less infrared excess than 21,500 K and because the model of Koester et al. (2005a) accounts for the measured high calcium abundance, while the Liebert et al. (2005) model does not.

Figure 10 shows a narrow ring model fitted to the infrared excess. To match the relatively low fractional luminosity of the disk, $\tau = 0.0006$, the model ring is narrow in radial extent and highly inclined. For a 20,400 K white dwarf, the inner and outer dust temperatures, in an optically thick disk, correspond to 19 and 21 stellar radii, or 0.25 and 0.28 $R_{\odot}$ respectively (Chiang & Goldreich 1997).

Due to the shape of the mild infrared excess at PG 1457−086, it is the only metal-rich white dwarf *Spitzer* target where a substellar companion might be considered as viable. If the measured $J = 16.07$ mag is solely due to the white dwarf photosphere, then the difference between the measured and model-predicted K-band flux for such a 20,000 K hydrogen white dwarf is $\Delta K = 0.24$ mag or an excess of $K = 17.8$ mag, which corresponds to $M_K = 12.6$ mag at the photometric distance of 110 pc (Liebert et al. 2005). If a self-luminous, substellar companion of this K-band brightness were orbiting PG 1457−086, it would have an effective temperature near 1500 K and a spectral type around L7 (Vrba et al. 2004; Dahn et al. 2002). It is worth noting that the white dwarf GD 1400 has an unresolved L7 brown dwarf companion, and the ratio of the 3.6 to 2.2 μm excess there is 1.3 (Farihi et al. 2005b), whereas for PG 1457−086 this value is 0.7, although these ratios are consistent within

the uncertainties.

As mentioned in the Appendix, winds from nearby M dwarf companions can, and occasionally do, pollute the atmospheres of white dwarfs. But for PG 1457−086 an M dwarf companion is ruled out by the absence of significant near-infrared excess (Farihi et al. 2005a). As described in the Appendix, there is no known connection between brown dwarf companions and the presence of metal pollution in white dwarf photospheres. Therefore, for PG 1457−086 to be metal-rich and to possess an L dwarf companion would require, simultaneously, two low probability events. For this reason, it is it highly unlikely that the excess infrared emission at PG 1457−086 is due to a brown dwarf companion.

3.3. LTT 8452

von Hippel et al. (2007) reported the discovery of *Spitzer* IRAC 4.5 and 7.9 μm excess due to warm dust at LTT 8452. Figure 7 shows the SED of this metal-rich white dwarf, now plotted with its IRAC 3.6, 5.7, and MIPS 24 μm data, which better constrain the inner and outer temperature of the disk. Figure 11 shows a flat ring model fitted to the mid-infrared emission of LTT 8452, with inner edge temperature $T_{\rm in} = 1000$ K, outer temperature $T_{\rm out} = 600$ K, and a modest inclination angle of $i = 53°$, whereas von Hippel et al. (2007) derived a temperature range of $900 - 550$ K and $i = 80°$. From the flat disk model, the fractional infrared luminosity of LTT 8452 is $\tau = 0.008$.

3.4. G238-44 and G180-57

Figure 4 includes all available *Spitzer* data for G238-44, one of the most highly contaminated, nearest, and brightest DAZ white dwarfs (Holberg et al. 1997). The aperture laid down for MIPS 24 μm photometry was extrapolated to the expected location of the star at the epoch 2007.3 observation, using the *Hipparcos* measured J2000 position and proper motion (Perryman et al. 1997). The expected position on the MIPS 24 μm array is in excellent agreement with the measured position of G238-44 in the epoch 2004.9 IRAC images, after accounting for proper motion, and coincides with a faint MIPS 24 μm source. However, the potential for source confusion is high.

If associated with the white dwarf, the Figure 4 apparent 24 μm excess at the location of G238-44 would be just slightly greater than 0.04 mJy (2.0σ). Based on *Spitzer* MIPS 24 μm source counts from deep imaging, the expected number of background galaxies of brightness 0.04 ± 0.02 mJy is around 8000 per square degree (Marleau et al. 2004). Hence within an

area of diameter equal to one full width at half maximum intensity at this wavelength (about 2.3 pixels or approximately 25 square arcseconds), there should be 0.015 galaxies of the right brightness to contaminate the MIPS aperture. Using a binomial probability, the chance of finding at least one in 20 metal-rich white dwarf targets confused with a background source in this manner is then 26%; therefore the 24 μm flux may not originate from G238-44.

Further, if the potential contamination area is widened to encompass two full widths at half maximum, the probability of source confusion is then 71%, although such a large an area is perhaps overly conservative. The expected position of G238-44 is offset from the centroid position of the MIPS source by 0.35 pixels or $0.9''$, the error of which is hard to estimate due to the relatively low S/N.

Turning to the white dwarf G180-57 (Figure 4), it has a 0.06 mJy (or 1.5σ excess) 24 μm source at its expected position on the array. All the previous arguments and caveats apply, and the chance that at least two in 20 MIPS targets are contaminated in this way is still relatively high, somewhere between 4% and 34%.

In any event, cold dust alone at this 24 μm luminosity level cannot explain the source of external metals in these white dwarfs. Blackbody dust which reveals itself at 24 μm but not at 8 μm would be around 200 K or cooler, and located too far away (at or beyond 10 and 70 $R_\odot$ for G180-57 and G238-44 respectively) to be the source of accreted metals in the photospheres of either white dwarf. Average-sized grains of 10 μm with density 2.5 g cm^{-3} at these distances would imply (minimum) dust masses around $10^{15} - 10^{17}$ g for $\tau = 10^{-5}$, appropriate for these detections, if real (Farihi et al. 2008b). This mass is insufficient to sustain an accretion rate of 3×10^8 g s^{-1} for more than 10 years at G238-44 (Koester & Wilken 2006).

3.5. vMa 2

The MIPS observations of vMa 2, plotted in Figure 1, suggest a 24 μm flux significantly lower than expected for a simple Rayleigh-Jeans extrapolation from its IRAC fluxes. Rather than an excess, the SED of vMa 2 appears deficient at 24 μm, at the 4σ level; the measured 24 μm flux is 0.11 ± 0.03 mJy, while the predicted flux is 0.23 mJy (Figure 1). Blackbody models are essentially no different than pure helium atmosphere white dwarf models at these long wavelengths (Wolff et al. 2002; see their Figure 1), hence the apparent deficit rests on the validity of the relatively low S/N photometry rather than model predictions. Still, this intriguing possibility requires confirmation with superior data, and if confirmed, vMa 2 would become by far the highest temperature white dwarf to display significant infrared flux

suppression due to collision-induced absorption (B. Hansen 2007, private communication; Farihi 2005).

3.6. Notes on Individual Objects

0108+277. NLTT 3915 belongs to an optical pair of stars separated by roughly $3''$ on the sky in a 1995.7 POSS II plate scan. The northeast star has proper motion $\mu = 0.22''$ yr^{-1} at $\theta = 222°$ (Lepine & Shara 2005) which can be readily seen between the POSS I and POSS II epochs. The IRAC images reveal two overlapping sources with a separation of $2.4''$ as determined by daophot at all four wavelengths. Using this task to deconvolve the pair of stars photometrically reveals the object to the southwest is likely a background red dwarf, based on its 2MASS and IRAC photometry, while the northeast star has colors consistent with a very cool white dwarf. Kawka & Vennes (2006) identified this star as a 5200 K DAZ white dwarf whose spectrum appears to exhibit sodium but not calcium; an anomalous combination for a metal-rich degenerate. Keck / HIRES observations confirm this object is a white dwarf, but with a cool DA spectrum and no metal features (C. Melis 2008, private communication). The data tables include fluxes, and the appendix gives limits on substellar companions for this target, but it is excluded it from analyses for metal-rich white dwarfs.

0208+396. G74-7 is the prototype DAZ star. IRAC observations of this white dwarf, previously reported in Debes et al. (2007) were taken during a solar proton event, and individual frames are plagued by legion cosmic rays, making the reduction and photometric analysis difficult, especially at the longer wavelengths. Only the 4.5 and 7.9 μm fluxes are plotted and tabled; some data were irretrievably problematic.

1202−232. This bright and nearby white dwarf is located about $8''$ away from a luminous infrared galaxy in the IRAC 8 μm images, and the white dwarf location is swamped by light from the galaxy at MIPS 24 μm, where the diffraction limit is $6''$. Hence the upper limit on the white dwarf 24 μm flux is about a factor of five worse than for a typical star.

1334+039. LHS 46 has been (mistakenly) identified as spectral type DZ in several papers over the years (Greenstein 1984; see discussion in Liebert 1977). It was first (correctly) re-classified as a DC star by Sion et al. (1990), and modern, high resolution spectroscopy confirms the white dwarf is featureless in the region of interest (Zuckerman & Reid 1998). Unfortunately, some relatively current literature (Holberg et al. 2008, 2002; McCook & Sion 1999) still contains the incorrect spectral type for this star and it was included in the *Spitzer* observations. The data tables include fluxes, and the appendix gives limits on substellar

companions for this target, but it is excluded it from analyses for metal-rich white dwarfs.

4. DISCUSSION

With the detection of mid-infrared excess at GD 16 and PG 1457−086, the number of externally polluted, cool white dwarfs with warm circumstellar dust becomes 14, including EC 1150−153 (Jura et al. 2009), SDSS 1228 (Brinkworth et al. 2008) (see Table 1), SDSS 1043 and Ton 345 (C. Brinkworth 2008, private communication; Melis et al. 2008). The latter three stars, whose photospheric metals and circumstellar gas disks were discovered simultaneously, are not analyzed here. Over 200 white dwarfs have been observed with *Spitzer* IRAC (Farihi et al. 2008a,b; Mullally et al. 2007; Debes et al. 2007; Hansen et al. 2006; Jura et al. 2007b; Friedrich et al. 2007). Of these, only stars with detected photospheric metals display an infrared excess, presumably because metal pollution from a circumstellar disk is inevitable and optical spectroscopy is a powerful tool for detecting the unusual presence of calcium in a white dwarf atmosphere. While the sample of white dwarfs observed with *Spitzer* is quite heterogeneous, it is likely that at least half of these stars have been observed in the Supernova Progenitor Survey (SPY; Napiwotzki et al. 2003), and hence with high sensitivity to photospheric calcium.

4.1. The Fraction of Single White Dwarfs with an Infrared Excess

The fraction of white dwarfs cooler than about 20,000 K that display photospheric metals depends on the stellar effective temperature and on whether its photospheric opacity is dominated by hydrogen or by helium. For DA white dwarfs, it is easier to detect metals in cooler stars and, in a survey that focused primarily on DA white dwarfs cooler than 10,000 K, Zuckerman et al. (2003) found that of order 25% displayed a calcium K line. In the extensive SPY survey, more focused on warmer white dwarfs with $T_{\rm eff} \gtrsim 10,000$ K, Koester et al. (2005a) found that only 5% show a calcium K line. To produce a detectable optical wavelength line at such high temperatures (and high opacities) typically requires a greater fractional metal abundance than at low temperatures. Because extensive ground and, especially, *Spitzer* surveys have failed to reveal infrared excess emission at any single white dwarf that lacks photospheric metals (Farihi et al. 2008b; Mullally et al. 2007; Hoard et al. 2007; Hansen et al. 2006; Farihi et al. 2005a), one can regard the above percentages as upper limits to the fraction of DA white dwarfs that possess dusty disks; at least until more sensitive metal abundance measurements can be achieved. Perhaps more instructive is the number DA stars without metals observed with *Spitzer*; 121 such targets

are reported between Mullally et al. (2007) and Farihi et al. (2008a), none of which show evidence for circumstellar dust, an upper limit of 0.8%.

Lower limits to the fraction of DA white dwarfs with dust disks can be estimated in the following way. Consider four large surveys of white dwarfs: the Palomar-Green Survey (347 DA stars; Liebert et al. 2005), the Supernova Progenitor Survey (478 DA stars; Koester et al. 2005a); the 371 white dwarfs from Farihi et al. (2005a), and the 1321 non-binary stars present in both the 2MASS (Hoard et al. 2007) and McCook & Sion (1999) catalogs. The presently known frequency of dust disks for white dwarfs in these four surveys, all of which tend to find warmer white dwarfs (due to luminosity), are 1.4, 1.5, 1.1 and 0.8%, respectively. Thus, because not all stars in these surveys have been searched for dust disks, one can say that, at a minimum, 1% of all warm white dwarfs have dust disks.

Spitzer surveys of cool metal-rich white dwarfs have now targeted 53 stars at $3 - 8$ μm using IRAC (a few at 4.5 and 7.9 μm only, but most at all wavelengths), while 31 of these targets have also been observed at 24 μm with MIPS (see Table 4). Including the unlikely exceptions discussed above, there does not exist a clear-cut case of MIPS 24 μm detection at any white dwarf without a simultaneous and higher IRAC flux – a telling result by itself. Hence, targets observed with IRAC only should accurately reflect the frequency of dusty degenerates.

Of the 53 contaminated white dwarfs surveyed specifically for circumstellar disks, 21% have mid-infrared data consistent with warm dust, regardless of atmospheric composition. With more data, this estimate is somewhat larger than the result of Kilic et al. (2008) that at least 14% of polluted white dwarfs have an infrared excess. As shown in Figure 12, the likelihood of a white dwarf displaying an infrared excess is strongly correlated with effective temperature and/or its measured calcium pollution. Only two of 34 stars with $T_{\text{eff}} \leq 10,000$ K have an excess, while that fraction is nine of 19 stars with $T_{\text{eff}} > 10,000$ K. Alternatively, nine (or ten) of 17 stars with $[\text{Ca/H(e)}] \geq -8.0$ possess an excess, whereas that fraction is only one (or two) of 38 stars with $[\text{Ca/H(e)}] < -8.0$.

4.1.1. The Role of Cooling Age

Cooling ages for the white dwarfs in Table 4 were calculated with the models of P. Bergeron (2002, private communication; Bergeron et al. 1995a,b). The white dwarf masses used as input for the cooling ages were taken from the literature (see Table 4 references), or $\log g = 8.0$ was assumed for those stars with no estimates available. Because cooling age is sensitive to mass, and because within the literature discrepancies exist among white

dwarf mass estimates, the values here should not be considered authoritative, but preference was given to values based on trigonometric parallaxes (Holberg et al. 2008) and those with multiple, independent, corroborating determinations. Still, it should be the case that a typical uncertainty in cooling age is between 10% and 20% due to an error in white dwarf mass.

Figure 12 indicates that the most metal-polluted white dwarfs are the warmest, and Figure 13 illustrates the same phenomenon, but now cast in terms of white dwarf cooling age. In the context of a model of tidal destruction of minor planets, as described below, it is plausible that younger (i.e., shorter cooling time) white dwarfs would be the most polluted. As indicated in the figure and tables, circumstellar dust disks are found at: eight of 17 stars (47%) with $t_{cool} < 0.5$ Gyr, two of 12 stars (17%) with 0.5 Gyr $< t_{cool} < 1.0$ Gyr, and only one of 24 (4%) stars with $t_{cool} > 1.0$ Gyr. The three dusty white dwarfs with cooling ages beyond 0.5 Gyr are: GD 362 and LTT 8452, both with cooling ages near 0.8 Gyr; and G166-58 with cooling age 1.29 Gyr.

To estimate the percentage of white dwarfs with cooling ages less than 0.5 Gyr that might have dusty disks, one can consider each of the four large surveys mentioned in the previous section. For example, the SPY survey contains 14 metal-contaminated DA white dwarfs with likely cooling ages less than 0.5 Gyr ($T_{eff} \gtrsim 11,000$ K). Of these 14, eight have been observed with IRAC and six have dust disks, while the remaining six, unobserved stars are prime candidates for dust disks (see §4.2). The SPY sample contains approximately 400 DA stars in this range of cooling ages and therefore, based on these data, it is likely that between 2% and 3% of white dwarfs with $t_{cool} < 0.5$ Gyr have detectable dust disks. This estimate is also consistent with the 72 DB white dwarfs (all with $T_{eff} \gtrsim 11,000$ K) observed with SPY (Voss et al. 2007; Koester et al. 2005b), two of which are metal-contaminated and possess dust disks.

In a similar manner, the SPY survey contains 10 metal-contaminated DA white dwarfs with likely cooling ages between 0.5 and 1.5 Gyr (7000 K $\lesssim T_{eff} \lesssim 11,000$ K). Of these 10, eight have been observed with IRAC and one has a dust disk, while the remaining two, unobserved stars both have [Ca/H] > -8.0, and hence one of them may have a disk. The SPY sample contains around 70 DA stars in this range of cooling ages, and therefore these data suggest between 1% and 2% white dwarfs with 0.5 Gyr $< t_{cool} < 1.5$ Gyr may have detectable dust disks. However, the smaller number statistics for these cooler white dwarfs make this estimate somewhat uncertain.

Assuming only metal-bearing white dwarfs can possess warm dust disks, the *Spitzer* observations suggest similar percentages. The fraction of younger, $t_{cool} < 0.5$ Gyr white dwarfs with dust disks can be estimated by observing the fraction of these with IRAC excess

is 0.47, and the fraction of SPY DA white dwarfs with metals in this cooling age range is 0.05, leading to a frequency between 2% and 3%, consistent with the above estimate. For somewhat older white dwarfs where 0.5 Gyr $< t_{\rm cool} <$ 1.5 Gyr, the same fractions are 0.10 with IRAC excess, and 0.13 with metal lines among SPY DA targets, yielding a frequency of 1%. For white dwarfs with $t_{\rm cool} >$ 1.5 Gyr, there there are not enough stars in appropriate age bins to make meaningful estimates.

Holberg et al. (2008) have compiled a nearly (estimated at 80%) complete catalog of white dwarfs within 20 pc of the Sun. In this local volume, there are 24 white dwarfs with 10,000 K $< T_{\rm eff} \lesssim 20,000$ K, and at least one white dwarf (G29-38), i.e. 4%, has an infrared excess. If the true percentage of warm dusty white dwarfs is 2.5%, then out to 50 pc there should be nine such stars with infrared excess. Currently, only GD 16 and GD 133 meet these criteria; either this expectation is incorrect or several white dwarfs within 50 pc of the Sun with an infrared excess remain to be discovered.

4.1.2. Implications for Disk Lifetimes and Pollution Events

The relative dearth of dust disks at the cooler metal-rich white dwarfs, as established by *Spitzer* observations, suggests that dust disk lifetimes are likely to be shorter than a typical $10^4 - 10^6$ yr heavy element diffusion timescale in either a hydrogen or helium atmosphere white dwarf at these temperatures. Whether a typical disk mass is fully consumed within that period or is rendered gaseous via collisions on much shorter timescales is unclear, and both mechanisms are likely to play a role to remove dust at white dwarfs (Jura 2008; Farihi et al. 2008b; Jura et al. 2007a). However, as noted above, the lack of dust at the cooler polluted stars is also related to their lower overall metal abundances, and partially an observational bias.

More important, this empirical result may have implications for the timescales of the events which give rise to and/or sustain circumstellar dust. If stochastic perturbations within a reservoir of planetesimals are the ultimate source of pollution events in metal-enriched white dwarfs, gradual depletion could give rise to a exponential decay in the number of events per unit time (Jura 2008), and hence the likelihood of a pollution event decreases as a white dwarf ages. Such a scenario is consistent with the *Spitzer* observations of the cooler, metal-lined white dwarfs, and would predict that the frequency of disruption, and subsequent disk creation events increases with increasing stellar effective temperature, corresponding to younger post-main sequence ages.

For typical white dwarfs of log $g = 8.0$, it takes around 0.07 Gyr to cool to an effective

temperature of 20,000 K, about 0.2 Gyr to 15,000 K, and just over 0.6 Myr to achieve 10,000 K (Bergeron et al. 1995a,b). The only known disk-bearing white dwarf which is likely to have a cooling age significantly older than several hundred Myr is G166-58; at 7400 K and assuming log g = 8.0, its cooling age should be near 1.3 Gyr. Notably, the properties of G166-58 are rather anomalous compared to the other known disk-bearing white dwarfs: its infrared excess comes up at 5 μm (Farihi et al. 2008a), while it has a modest calcium abundance and accretion rate. One possibility is that planetary system remnants at white dwarfs tend to stabilize by roughly 1 Gyr. Minor planet belts may become significantly depleted on these timescales or gravitational perturbations may subside on shorter timescales via dynamical rearrangement (Jura 2008; Bottke et al. 2005; Debes & Sigurdsson 2002).

On the other hand, the lack of dust at the relatively warm, but highly polluted white dwarf HS 2253+803 points to a disk lifetime shorter than the timescale for removal of accreted metals. This very metal-enriched and carbon-poor degenerate sits in the outlying region of Figure 12 where it is virtually the only star in this abundance range without a disk. Therefore, it is likely this star had a dust disk which has been fully consumed within the 10^6 yr diffusion timescale for this warm DBAZ.

4.2. Metal Accretion Rates

It has been previously argued that DAZ white dwarfs with the highest calcium abundances also have an infrared excess and, thus, a circumstellar disk (Kilic et al. 2006). This argument has been slightly recast (Jura et al. 2007b; Jura 2008) to suggest that those DAZ white dwarfs with the highest metal accretion rates are the stars with infrared excess. However, put into this proper context, both DAZ and DBZ white dwarfs should exhibit this correlation, if correct. This connection between disk frequency and metal accretion rate is now re-evaluated for all 53 metal-polluted white dwarfs observed with the IRAC camera.

Assuming accretion-diffusion equilibrium (i.e. a steady state), mass accretion rates were calculated using Equation 2 of Koester & Wilken (2006) with the best available photospheric calcium abundance determinations, together with the solar calcium abundance relative to either hydrogen or helium, as appropriate. Settling times for various metals are usually within a factor of 2 (Koester & Wilken 2006; Dupuis et al. 1993), and calcium is employed here because it is the best studied element. Where available for DAZ stars, convective envelope masses and calcium diffusion timescales were taken from Table 3 of Koester & Wilken (2006). Otherwise log g = 8 was assumed and diffusion timescales were taken directly from their Table 2, while convective envelope masses were interpolated using their Table 3 values for stars of similar effective temperature and surface gravity (log g = 8 was also assumed for

G166-58 for reasons discussed in Farihi et al. 2008b). For DBZ stars, convective envelope masses were read from Figure 1 of Paquette et al. (1986), and calcium diffusion times were interpolated using their Table 2 values; all assuming $M = 0.6\ M_\odot$.

In actuality, steady state accretion is likely for the warmer DAZ stars, but much less so for the cooler DAZ and DBZ stars, which have relatively long metal dwell times. Based on this work and the results of Kilic et al. (2008), it is likely that disks at white dwarfs typically dissipate within $10^4 - 10^5$ yr, a timescale at which photospheric metals persist in the cooler DAZ and DBZ stars. Hence, the calculated accretion rates listed in Table 4 should be considered *time-averaged* over a single diffusion timescale, and may not accurately describe stars where detectable metals may dwell beyond 10^3 yr. An additional factor of $1/100$ was introduced to "correct" the Koester & Wilken (2006) Equation 2 rates to reflect that only accreted heavy elements are of interest, this factor being the typical dust-to-gas ratio in the interstellar medium. Figure 14 plots these accretion rates for all *Spitzer* observed stars versus effective temperature. Figure 15 plots the same metal accretion rates versus white dwarf cooling age.

The results show that the implied metal accretion rates are quite similar between the two atmospheric varieties of metal-rich white dwarf, strengthening the argument that their externally-polluted photospheres are caused by a common phenomenon; namely circumstellar material. In fact, at accretion rates $dM/dt \gtrsim 3 \times 10^8$ g s^{-1}, the fraction of metal-rich white dwarfs with circumstellar dust – regardless of atmospheric composition – is over 50%. If one associates accretion rate with circumstellar disk mass (a modest assumption), then this picture is consistent with white dwarf dust disks being strongly linked to tidal disruption events involving fairly large minor planets; while less massive disrupted asteroids give rise to more tenuous (possibly shorter-lived, possibly gaseous) disks, and modest accretion rates.

While the white dwarfs with an infrared excess are likely accreting from tidally-disrupted minor planets, the origin of the pollution in high accretion rate white dwarfs without obvious evidence for a disk is uncertain. Jura (2008) has proposed that if multiple, small asteroids are tidally-disrupted, their debris self-collides so the dust is efficiently destroyed, and matter then accretes onto the white dwarf from an undetected gaseous disk. Given that the typical timescale for collisions within a white dwarf dust disk is hours, with disk velocities at hundreds of km s^{-1}, it is also conceivable that a single, modest-sized planetesimal could grind itself down to gas-sized material via self-collisions (Farihi et al. 2008b). Another possibility is that the dwell time of the photospheric metals in the white dwarf is longer than the characteristic disk dissipation time (Kilic et al. 2008).

4.3. Circumstellar Versus Interstellar Accretion

Two competing models to explain the metal-contaminated photospheres of white dwarfs involve interstellar accretion and circumstellar accretion (Sion et al. 1990; Alcock et al. 1986). The SEDs of the mid-infrared excess at GD 16 and PG 1457−086 are well explained by a circumstellar dust disk arising from a tidally disrupted asteroid or similar planetesimal, but are not consistent with interstellar accretion. The same argument applies to the other metal-rich white dwarfs with mid-infrared excess; simply stated, the compact size and olivine composition of the dust are at odds with expectations for disks formed through interstellar accretion (Jura et al. 2007a,b; Reach et al. 2005).

With Equation 3 of Jura et al. (2007a) and following their method, predicted 24 μm fluxes were calculated for all 32 metal-rich white dwarfs observed with MIPS, assuming interstellar Bondi-Hoyle type grain accretion followed by Poynting-Robertson drag onto the star. Figure 16 displays these predicted infrared fluxes from interstellar accretion versus the MIPS 24 μm upper limits for 25 white dwarfs; stars with fluxes consistent with circumstellar disks were excluded, as were targets with contaminated photometry. The plot shows that the predicted fluxes are typically more than an order of magnitude greater than the observed 3σ upper limits. With few possible exceptions, this simple interstellar accretion model cannot account for the observed infrared data.

Furthermore, there is now a growing number of DB white dwarfs with evidence for external pollution via carbon deficiency, relative to metals such as iron (Desharnais et al. 2008; Zuckerman et al. 2007; Jura 2006; Wolff et al. 2002). They have accreted rocky material, independent of any evidence for or against circumstellar dust. Table 5 lists the seven known helium- and metal-rich white dwarfs with low carbon abundances or upper limits. Of these stars, only two of six observed by *Spitzer* have strong evidence in favor of circumstellar dust, GD 40 and GD 362. This raises the possibility that the remaining dust-poor and metal-rich stars are accreting gaseous heavy elements.

Figure 14 reveals that the DBZ HS 2253+803 has one of the highest implied (time-averaged) accretion rates among all polluted white dwarfs, yet has no dust disk as evidenced by the *Spitzer* photometry presented here. This white dwarf is spectacularly carbon-poor relative to its metal content, and is highly likely to have accreted rocky material (Jura 2006). In this particular case, its near pure helium nature gives it a likely diffusion timescale of 10^6 yr, and hence a dissipated disk is quite possible; yet its atmospheric metal composition should nonetheless provide a measure of the extrasolar planetary material it has accreted.

The preponderance of the evidence firmly favors the interpretation that heavily metal-contaminated white dwarfs are currently accreting, or have in their recent history accreted,

rocky planetesimal material in either dusty or gaseous form. The origin of the metals in white dwarfs at the low end of [Ca/H(e)] ratios and metal accretion rates, such as a number of DAZs in the survey of Zuckerman et al. (2003) remains unclear.

4.4. Comparison with Main-Sequence Stars with Planetary Systems

The circumstellar disks around white dwarfs likely arise from the tidal disruption of minor planets, with inferred metal accretion rates $dM/dt \gtrsim 3 \times 10^8$ g s^{-1}. In the solar system, the dust production rate in the zodiacal cloud is near 10^6 g s^{-1} (Fixsen & Dwek 2002). Collisions among parent bodies result in dust production rates around main-sequence A-type stars in excess of 10^{10}g s^{-1} (Chen et al. 2006). Thus, the rate estimated for the erosion of minor planets around white dwarfs is within the range inferred for main-sequence stars. Because A-type stars evolve into white dwarfs, it appears there is an ample population of parent bodies among the main-sequence progenitors of white dwarfs to account for the observed pollutions.

The model in which an infrared excess around a white dwarf results from a tidally-disrupted minor planet requires that the orbit of an asteroid is perturbed substantially (Debes & Sigurdsson 2002). It is plausible that a Jupiter-mass planet is such a perturber. Cumming et al. (2008) find that 10.5% of solar-type stars have gas giant planetary companions with periods between two and 2000 dy. Clearly, many of these planets will be destroyed when the main-sequence star becomes a first ascent and then asymptotic giant (Farihi et al. 2008a), but half of these planets have periods longer than one year and may survive. At present, the known fraction of main-sequence stars with massive planets that could persist beyond the post-main sequence evolution of their host is comparable to the estimated fraction of white dwarfs with an infrared excess. The upper mass limits for self-luminous companions to white dwarfs, as found by this and previous *Spitzer* studies, are consistent with the scenario that asteroid orbits are perturbed by a typical gas giant planet (Farihi et al. 2008a,b).

5. CONCLUSIONS

Spitzer mid-infrared observations of metal-contaminated white dwarfs are extended to a larger sample, and to longer wavelengths, including numerous DBZ targets. This study builds on previous work which all together indicate that warm dust orbits 21% of all externally polluted white dwarfs observed by *Spitzer*. Several patterns are revealed among the

degenerates with and without warm circumstellar dust, which together lend support to the idea that tidally disrupted planetesimals are responsible for the heavy element abundances in many, if not most externally polluted white dwarfs.

1. Sufficient metal-rich targets now have been studied to estimate that between 1% and 3% of single white dwarfs with cooling ages less than around 0.5 Gyr possess an infrared excess that is likely the result of a tidally-disrupted asteroid. Evidence is strong that white dwarfs can be used to study disrupted minor planets.

2. As yet no evidence for cool, $T < 400$ K dust exists from MIPS 24 μm observations of more than 30 metal-rich white dwarfs, including many with heavily polluted photospheres. All stars with circumstellar disks detected at 24 μm have coexisting, strong $3 - 8$ μm IRAC excess fluxes. The disks appear outwardly truncated; their mid-infrared spectral energy distributions are clearly decreasing at wavelengths beyond 8 μm. These observed and modeled infrared excesses indicate rings of dust where the innermost grains typically exceed $T = 1000$ K, and outer edges which lie within the Roche limit of the white dwarf, consistent with disks created via tidal disruption of rocky planetesimals.

3. Circumstellar disks at white dwarfs are vertically optically thick at wavelengths as long as 20 μm. Particles in an optically thin disk would not survive Poynting-Robertson drag for more than a few days to years. Additionally, the warmest dust has been successfully modeled to lay within the radius at which blackbody grains in an optically thin cloud should sublimate rapidly. With a single, notable exception (G166-58), the dusty circumstellar disks have inner edges which approach the sublimation region for silicate dust in an optically thick disk; precisely the behavior expected for a dust disk which is feeding heavy elements to the photosphere of its white dwarf host.

4. The majority of metal-contaminated white dwarfs do not have dust disks. Circumstellar gas disks are a distinct possibility at dust-free, metal-rich stars with $dM/dt \geq 3 \times 10^8$ g s^{-1}. Fully accreted disks are a possibility for white dwarfs with metal diffusion timescales approaching 10^6 yr. It is possible that a critical mass and density must be reached to prevent the dust disk from rapid, collisional self-annihilation, and when this milestone is not reached, a gas disk results. If correct, optical and ultraviolet spectroscopy of metal-rich white dwarfs are powerful tools with which to measure the bulk composition of extrasolar planetary material.

5. Cooling age is correlated with the frequency of dusty disks at white dwarfs; for $T_{\rm eff} \lesssim 20,000$ K, white dwarfs with younger cooling ages are more likely to be orbited by a dusty disk. G166-58 is by far the coolest white dwarf with a (rather anomalous) infrared excess, and the timescale for diffusion of metals out of the photosphere is relatively long for

a DAZ white dwarf.

Spitzer IRAC may soon bring a few more dust discoveries at polluted white dwarfs, but the statistics are unlikely to change significantly without a commensurate increase in the number of surveyed stars. Such a program remains feasible with IRAC in the post-cryogenic phase, provided that $T \sim 1000$ K dust is present in most white dwarf circumstellar disks. Unfortunately, objects with somewhat cooler dust emission such as G166-58 will evade detection until *JWST*, which should have photometric sensitivity similar to, or better than, *Spitzer* at all relevant mid-infrared wavelengths. Observations of a sizable number of metal-contaminated white dwarfs at longer wavelengths, where cold planetesimal belt debris might be seen *in situ*, will have to await future facilities. If belts of rocky planetary remnants persist around metal-polluted white dwarfs at tens of AU, where Poynting-Robertson drag cannot remove large particles within 10^9 yr, then sensitive submillimeter observations may have a chance to directly detect them.

Facility: Spitzer (IRAC,MIPS)

A. IRAC CONSTRAINTS ON THE PRESENCE OF SUBSTELLAR COMPANIONS TO METAL-RICH WHITE DWARFS

An assessment of the presence of substellar companions to the metal-rich white dwarfs in this work and in Jura et al. (2007a) is made below via IRAC data. Limits on unresolved substellar companions are placed at 23 metal-rich white dwarfs from IRAC 4.5 μm photometry and current models.

A.1. Limits for Unresolved Substellar Companions

In addition to circumstellar dust, IRAC observations are sensitive to unresolved substellar companions at white dwarfs, via photometric excess (Farihi et al. 2008a; Mullally et al. 2007; Debes et al. 2007; Hansen et al. 2006; Farihi et al. 2005b). Moreover, there exist a

few metal-enriched white dwarfs which reside in close, detached, binaries with unevolved M dwarfs; in such systems, the source of the photospheric pollutants is thought to be the stellar wind of the main sequence companion (Zuckerman et al. 2003). Therefore, it is reasonable to ask if previously unseen, close, substellar companions might be responsible for the heavy elements in some contaminated white dwarfs.

Externally polluted white dwarfs observed with IRAC at 4.5 μm, but without obvious photometric excess due to circumstellar dust, and not previously analyzed for substellar companions, were selected from this study as well as from Jura et al. (2007a) and Mullally et al. (2007), yielding a total of 23 targets. All data were analyzed independently as described in §2. Following the technique of Farihi et al. (2008b), the absolute magnitude of a substellar companion with a putative 3σ photometric excess (above the observed flux) at 4.5 μm was determined using their Equation 2. This magnitude was translated into a mass based on a calculated total (main sequence plus cooling) age for each white dwarf, utilizing appropriate substellar evolutionary models (I. Baraffe 2007, private communication; Baraffe et al. 2003).

Table 6 lists the main sequence lifetime, $t_{\rm ms}$, cooling age, $t_{\rm cool}$, distance from Earth, absolute 4.5 μm magnitude brightness limit and corresponding companion upper mass limit, for each metal-rich white dwarf. Combined with previous results for 20 similar IRAC targets (16 from Farihi et al. 2008a; four from Debes et al. 2007), there are now 43 cool contaminated white dwarfs observed with IRAC and analyzed for substellar companions; none show evidence for closely orbiting, potentially polluting secondaries down to an average mass of 19 ± 8 $M_{\rm J}$. The hypothesis that unseen, brown dwarf companions are the source of heavy elements in some white dwarf atmospheres is essentially ruled out by these observations.

A.2. Limits for Resolved Substellar Companions

Again, following the methodology of Farihi et al. (2008a), upper mass limits were established for spatially resolved (widely bound) T and sub-T dwarf companions for eight white dwarfs within $d \approx 20$ pc. These upper mass limits ($M_{\rm J}$, Table 7) are considerably higher (average of 60 $M_{\rm J}$) than those for unresolved companions at the same stars, due to the criteria that they must be well-detected at all four IRAC channels (Farihi et al. 2008a).

REFERENCES

Alcock, C., Fristrom, C. C., & Siegelman, R. 1986, ApJ, 302, 462

Baraffe, I., Chabrier, G., Barman, T. S., Allard, F., & Hauschildt, P. H. 2003, A&A, 402, 701

Becklin, E. E., Farihi, J., Jura, M., Song, I., Weinberger, A. J., & Zuckerman, B. 2005, ApJ, 632, L119

Bergeron, P., Saumon, D., & Wesemael, F. 1995a, ApJ, 443, 764

Bergeron, P., Wesemael, F., & Beauchamp, A. 1995b, PASP, 107, 1047

Bottke, W. F., Durda, D. D., Nesvorný, D., Jedicke, R., Morbidelli, A., Vokrouhlický, D., & Levison, Hal 2005. Icarus, 175, 111

Brinkworth, C. S., Gänsicke, B. T., Marsh, T. R., Hoard, D. W., & Tappert, C. 2009, ApJ, in press

Burleigh, M. R., Hogan, E., Dobbie, P. D., Napiwotzki, R., Maxted, P. F. L. 2006, MNRAS, 373, L55

Chen, C. H., et al. 2006, ApJS, 166, 351

Chiang, E. I., & Goldreich, P. 1997, ApJ, 490, 368

Cumming, A., Butler, R. P., Marcy, G. W., Vogt, S. S., Wright, J. T., & Fischer, D. A. 2008, PASP, 120, 531

Dahn, C. C., et al. 2002, AJ, 124, 1170

Debes, J. H., & Sigurdsson, S. 2002, ApJ, 572, 556

Debes, J. H., Sigurdsson, S. & Hansen, B. 2007, AJ, 134, 1662

Desharnais, S., Wesemael, F., Chayer, P., Kruk, J. W., & Saffer, R. A. 2008, ApJ, 672, 540

Dufour, P., et al. 2007, ApJ, 663, 1291

Dupuis, J., Fontaine, G., & Wesemael, F. 1993b, ApJS, 87, 345

Engelbracht, C. W., et al. 2007, PASP, 119, 994

Farihi, J. 2005, AJ, 129, 2382

Farihi, J., Becklin, E. E., & Zuckerman, B. 2005a, ApJS, 161, 394

Farihi, J., Becklin, E. E., & Zuckerman, B. 2008a, ApJ, 681, 1470

Farihi, J., Zuckerman, B., & Becklin, E. E. 2005b, AJ, 130, 2237

Farihi, J., Zuckerman, B., & Becklin, E. E. 2008b, ApJ, 674, 431

Fazio, G. G., et al. 2004, ApJS, 154, 10

Fixsen, D. J., & Dwek, E. 2002, ApJ, 578, 1009

Friedrich, S., Koester, D., Heber, U., Jeffery, C. S., & Reimers, D. 1999, A&A, 350, 865

Friedrich, S., Zinnecker, H., Correia, S., Brandner, W., Burleigh, M. R., & McCaughrean, M. 2007, Proceedings of the 15th European Workshop on White Dwarfs, eds. M. R. Burlgeigh & R. Napiwotzki (San Francisco: ASP), 343

Gänsicke, B. T., Koester, D., Marsh, T. R., Rebassa-Mansergas, A., & Southworth J. 2008, MNRAS, 391 L103

Gänsicke, B. T., Marsh, T. R., Southworth, J., & Rebassa-Mansergas, A. 2006, Science, 314, 1908

Gänsicke, B. T., Marsh, T. R., & Southworth, J. 2007, MNRAS, 380, L35

Giclas, H. L., Burnham, R. T., & Thomas, N. G. 1965, Lowell Observatory Bulletin (Flagstaff: Lowell Observatory), 6, 155

Graham, J. R., Matthews, K., Neugebauer, G., & Soifer, B. T. 1990, ApJ, 357, 216

Greenstein, J. L. 1984, ApJ, 276, 602

Hansen, B. M. S., Kulkarni, S., & Wiktorowicz, S. 2006, AJ, 131, 1106

Hoard, D. W., Wachter, S., Sturch, L. K., Widhalm, A. M., Weiler, K. P., Pretorius, M. L., Wellhouse, J. W., Gibiansky, M. 2007, AJ, 134, 26

Holberg, J. B., Barstow, M. A., & Green, E. M. 1997, ApJ, 474, L127

Holberg, J. B., Oswalt, T. D., & Sion, E. M. 2002, ApJ, 571, 512

Holberg, J. B., Sion, E. M., Oswalt, T., McCook, G. P., Foran, S., & Subasavage, J. P. 2008, AJ, 135, 1225

Ida, S., & Lin, D. N. C. 2008, ApJ, 673, 487

Jura, M. 2003, ApJ, 584, L91

Jura, M. 2006, ApJ, 653, 613

Jura, M. 2008, AJ, 135, 1785

Jura, M., Farihi, J., & Zuckerman, B. 2007a, ApJ, 663, 1285

Jura, M., Farihi, J., & Zuckerman, B. 2009, AJ, in press

Jura, M., Farihi, J., Zuckerman, B., & Becklin, E. E. 2007b, AJ, 133, 1927

Kawka, A., & Vennes, S. 2006, ApJ, 643, 402

Kawka, A., Vennes, S., & Thorstensen, J R. 2004, AJ, 127, 1720

Kilic, M., Farihi, J., Nitta, A., & Leggett, S. K. 2008, AJ, 136, 111

Kilic, M., & Redfield, S. 2007, ApJ, 660, 641

Kilic, M., von Hippel, T., Leggett, S. K., & Winget, D. E. 2005, ApJ, 632, L115

Kilic, M., von Hippel, T., Leggett, S. K., & Winget, D. E. 2006, ApJ, 646, 474

Koester, D., & Wilken, D. 2006, A&A, 453, 1051

Koester, D., Rollenhagen, K., Napiwotzki, R., Voss, B., Christlieb, N., Homeier, D., & Reimers, D. 2005a, A&A, 432, 1025

Koester, D., Napiwotzki, R., Voss, B., Homeier, D., & Reimers, D. 2005b, A&A, 439, 317

Lepine, S., & Shara, M. M. 2005, AJ, 129, 1483

Liebert, J. 1977, A&A, 56, 427

Liebert, J., Bergeron, P., & Holberg, J. B. 2005, ApJS, 156, 47

Marleau, F. R., et al. 2004, ApJS, 154, 66

McCook, G. P., & Sion, E. M. 2006, Catalog of Spectroscopically Identified White Dwarfs (Strasbourg: CDS)

McCook, G. P., & Sion, E. M. 1999, ApJS, 121, 1

Melis, C., Zuckerman, B., Albert, L., Jura, M., & Klein, B. 2008, ApJ, submitted

Monet, D., et al. 2003, AJ, 125, 984

Mullally, F., Kilic, M., Reach, W. T., Kuchner, M. J., von Hippel, T., Burrows, A., & Winget, D. E. 2007, ApJS, 171, 206

Napiwotzki, R., et al. 2003, Msngr, 112, 25

Paquette, C., Pelletier, C., Fontaine, G., & Michaud, G. 1986, ApJS61, 197

Perryman, M. A. C., et al. 1997, A&A, 323, L49

Probst, R. 1983, ApJS, 53, 335

Reach, W. T., Kuchner, M. J., von Hippel, T., Burrows, A., Mulally, F., Kilic, M., & Winget, D. E. 2005, ApJ, 635, L161

Rieke, G., et al. 2004, ApJS, 154, 25

Salim, S., & Gould, A. 2003, ApJ, 582, 1011

Sion, E. M., Hammond, G. L., Wagner, R. M., Starrfield, S. G., & Liebert, J. 1990, ApJ, 362, 691

Skrutskie, M. F., et al. 2006, AJ, 131, 1163

von Hippel, T., Kuchner, M. J., Kilic, M., Mullaly, F., & Reach, W. T. 2007, ApJ, 662, 544

Voss, B., Koester, D., Napiwotzki, R., Christlieb, N., & Reimers, D. 2007, A&A, 470, 1079

Vrba, F., et al. 2004, AJ, 127, 2948

Wolff, B., Koester, D., & Liebert, J. 2002, A&A, 385, 995

Zuckerman, B. 2001, ARA&A, 39, 549

Zuckerman, B., & Becklin, E. E. 1987a, ApJ, 319, 99

Zuckerman, B., & Becklin, E. E. 1987b, Nature, 330, 138

Zuckerman, B., Koester, D., Melis, C., Hansen, B. M. S., & Jura, M. 2007, ApJ, 671, 872

Zuckerman, B., Koester, D., Reid, I. N., & Hünsch, M. 2003, ApJ, 596, 477

Zuckerman, B., & Reid, I. N. 1998, ApJ, 505, 143
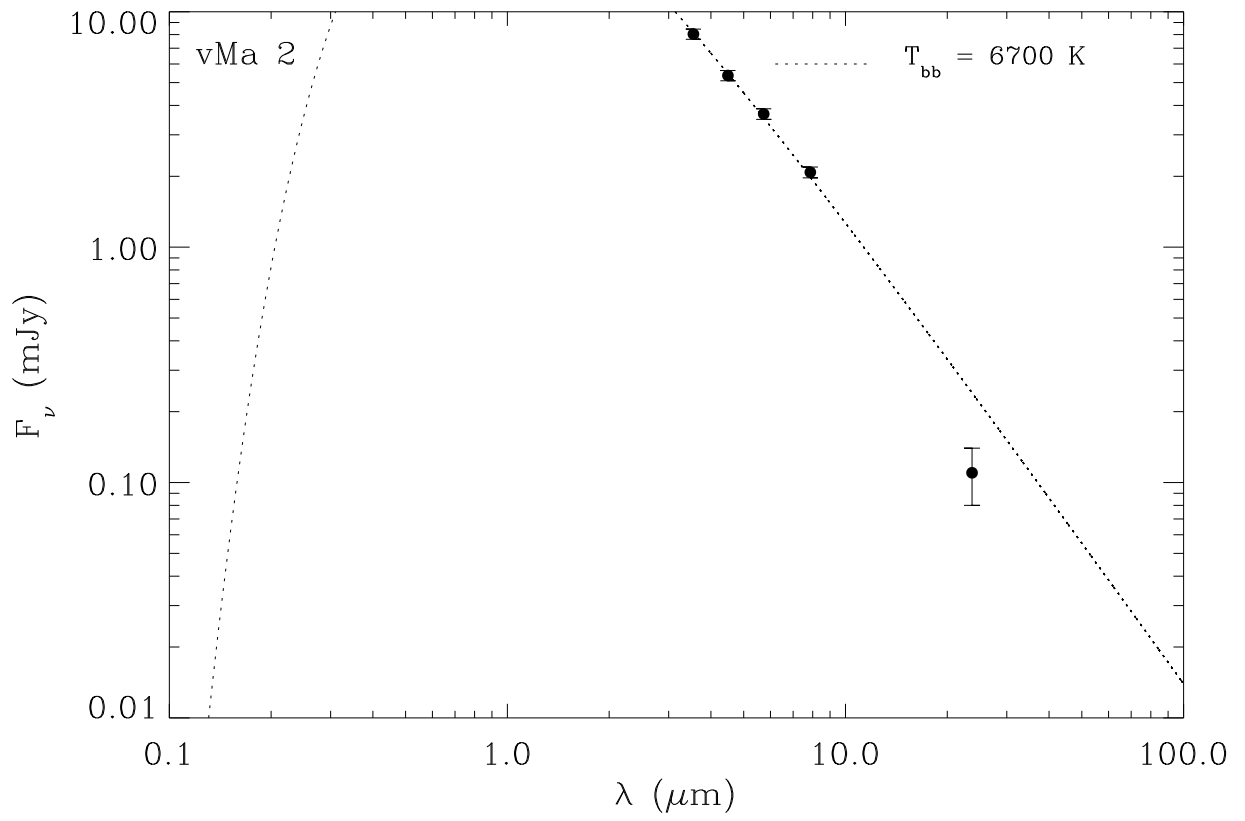
Fig. 1.— SED of vMa 2.
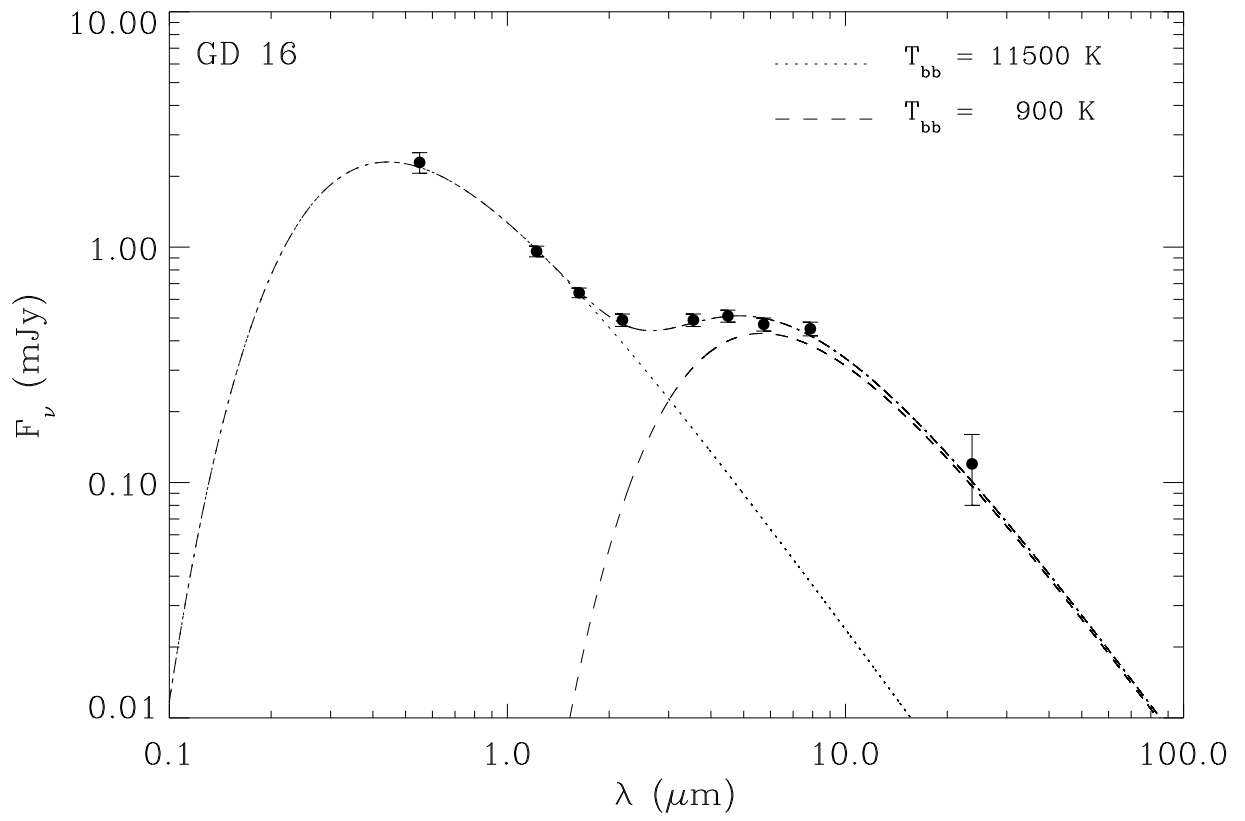
Fig. 2.— SED of GD 16.
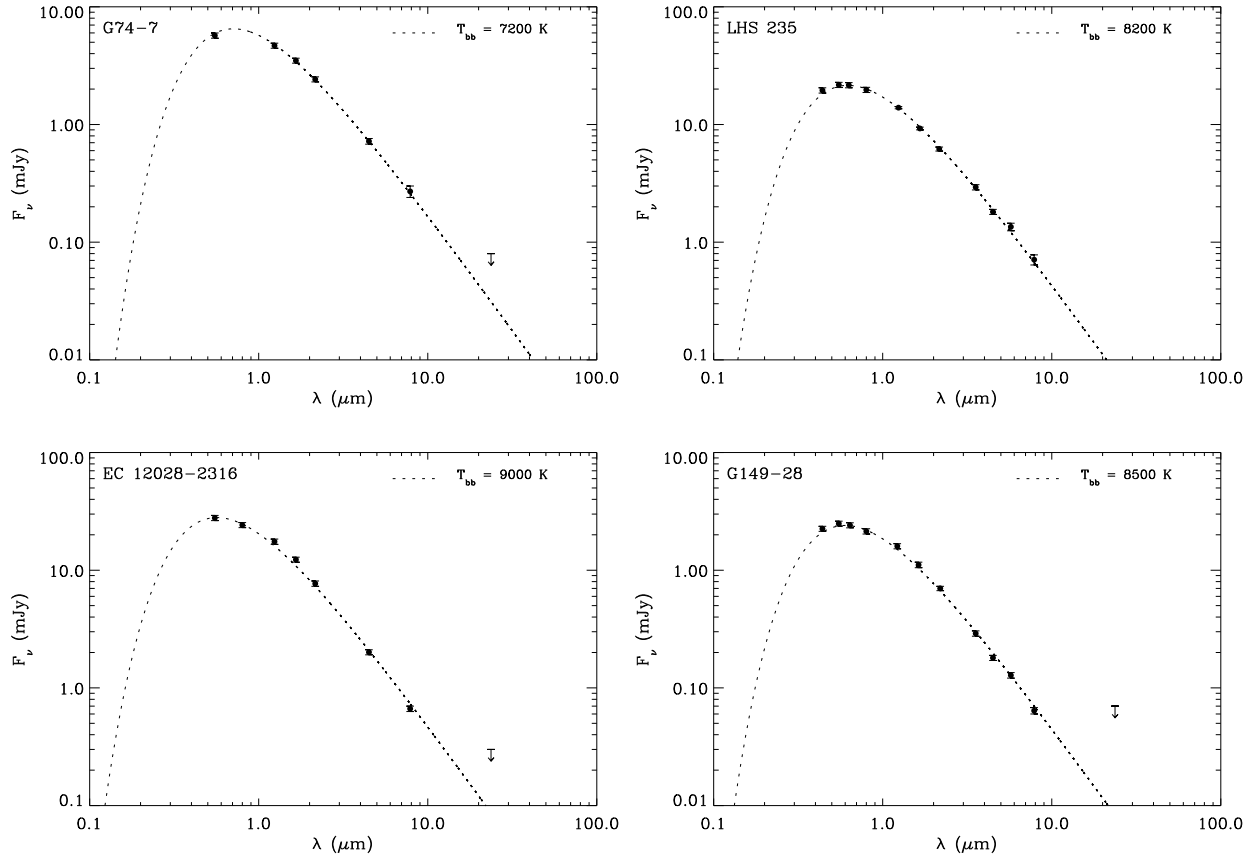
Fig. 3.— SEDs of G74-7, LHS 235, EC 1202−232, and G149-28. Downward arrows represent 3σ upper limits (§2).
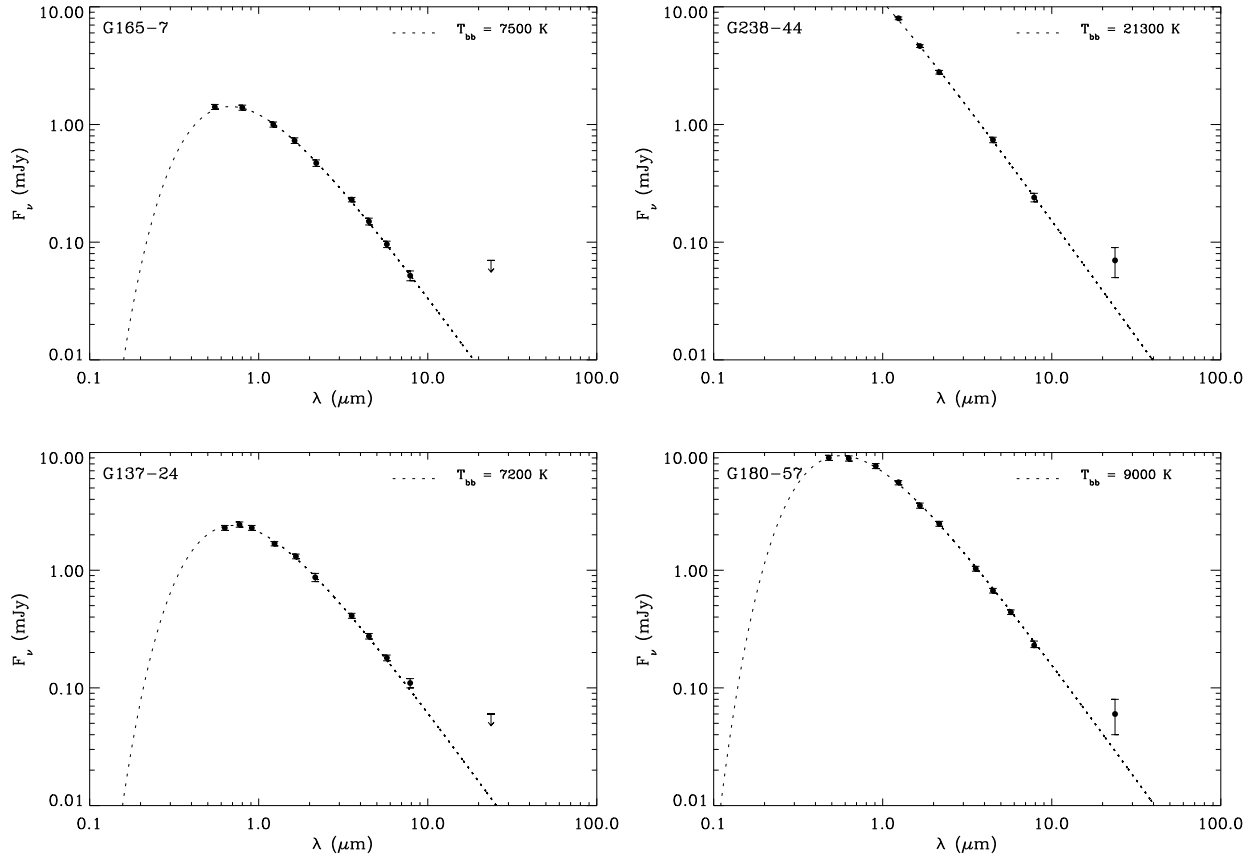
Fig. 4.— SEDs of G165-7, G238-44, G137-24, and G180-57. Downward arrows represent 3σ upper limits (§2).
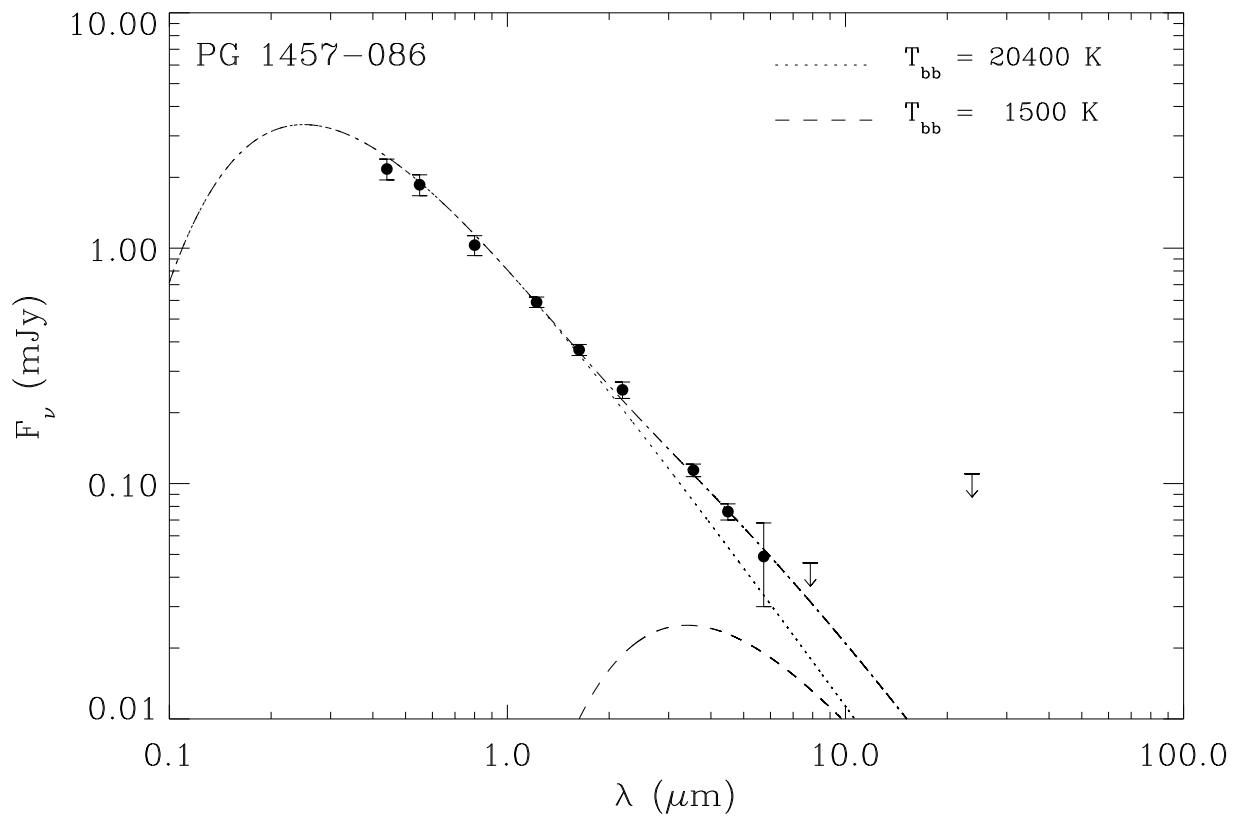
Fig. 5.— SED of PG 1457−086. Downward arrows represent 3σ upper limits (§2).
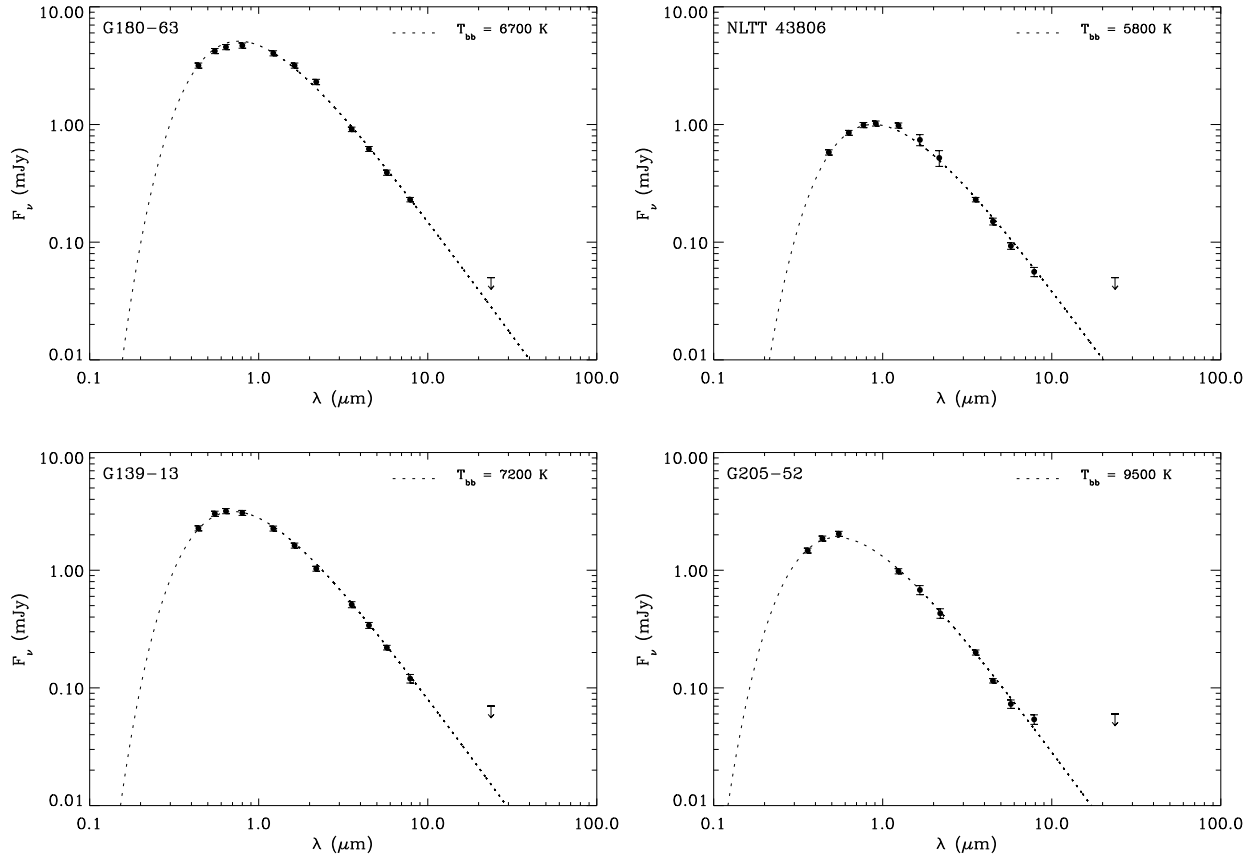
Fig. 6.— SEDs of G180-63, NLTT 43806, G139-13, and G205-52. Downward arrows represent 3σ upper limits (§2).
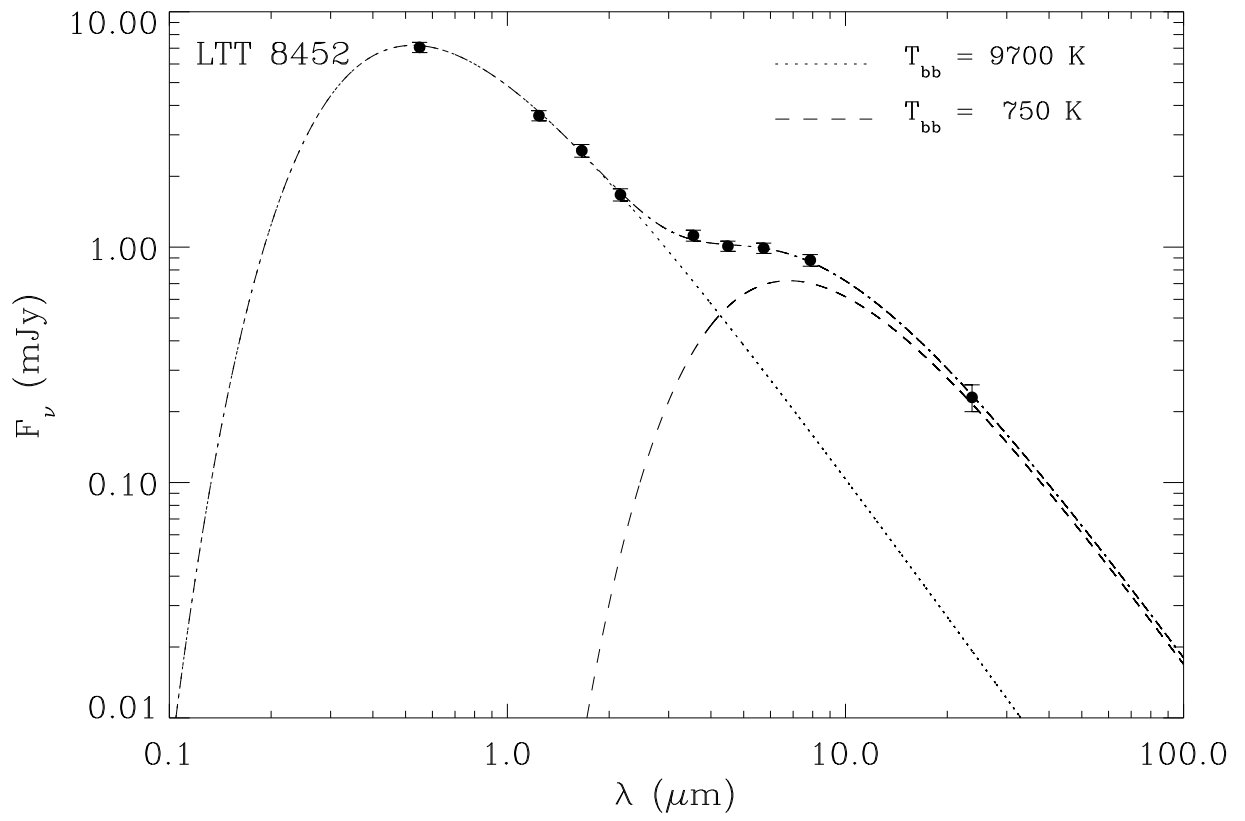
Fig. 7.— SED of LTT 8452.
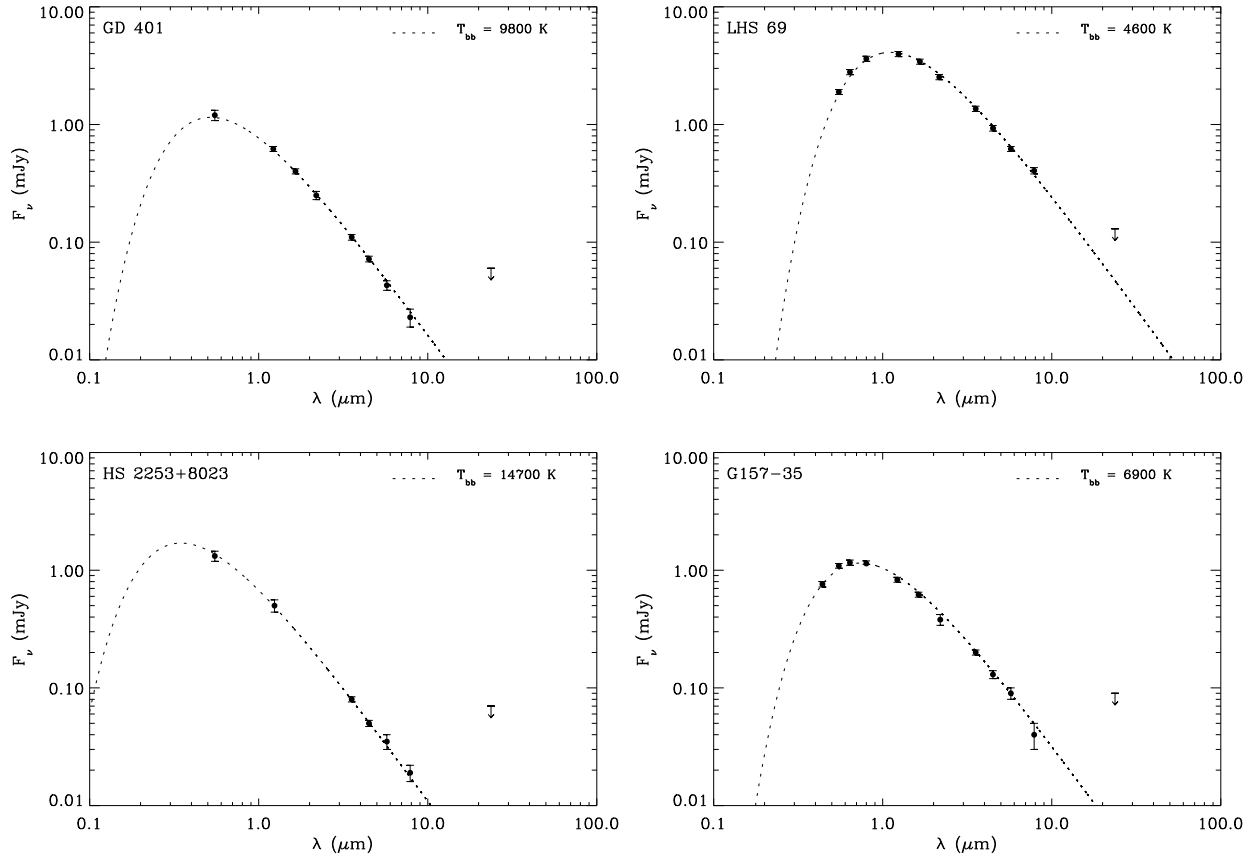
Fig. 8.— SEDs of GD 401, LHS 69, HS 2253+8023, and G157-35. Downward arrows represent 3σ upper limits (§2).
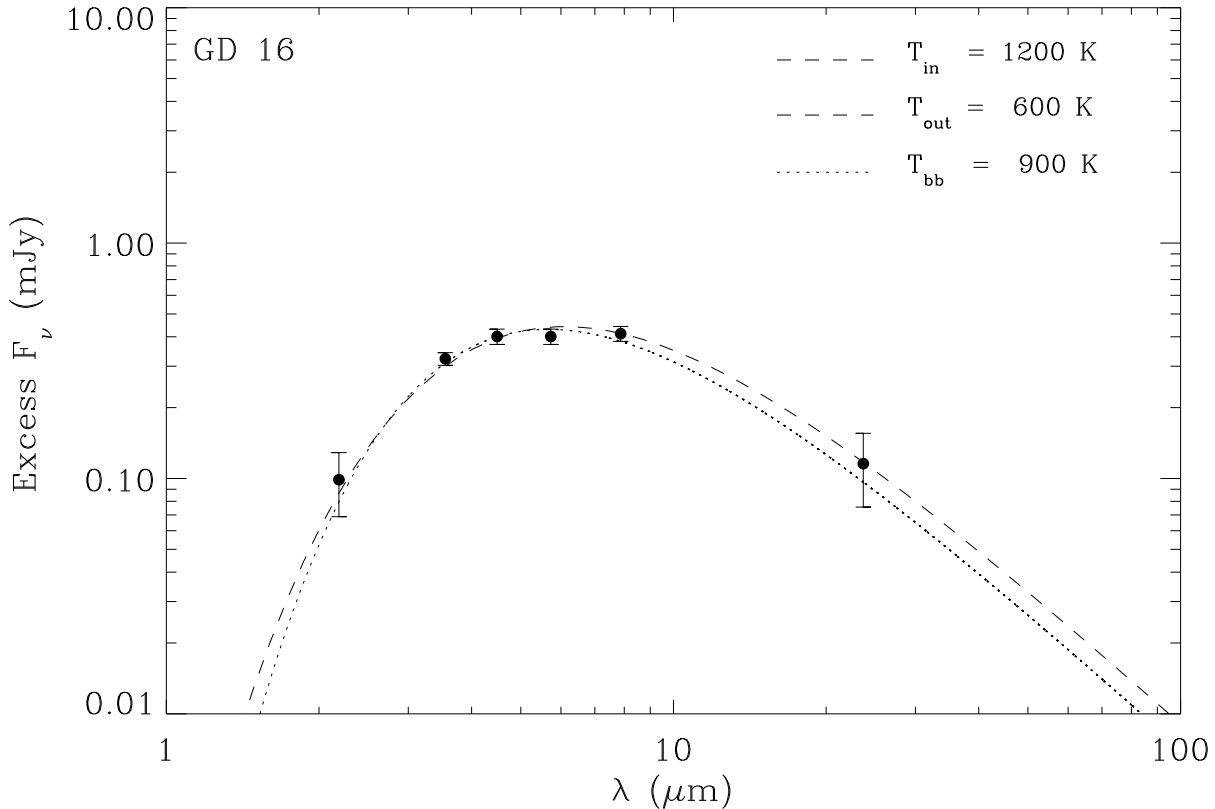
Fig. 9.— Excess infrared emission above the stellar photosphere from GD 16 fitted with a model circumstellar disk. The dashed line represents an optically thick, geometrically thin disk of inclination angle $i = 48°$ ($i = 0°$ is face-on) and finite radial extent, whose inner edge temperature is $T_{in} = 1200$ K and whose outer temperature is $T_{out} = 600$ K (Jura 2003). As may be seen, emission from a 900 K blackbody is a close approximation to the model ring emission.
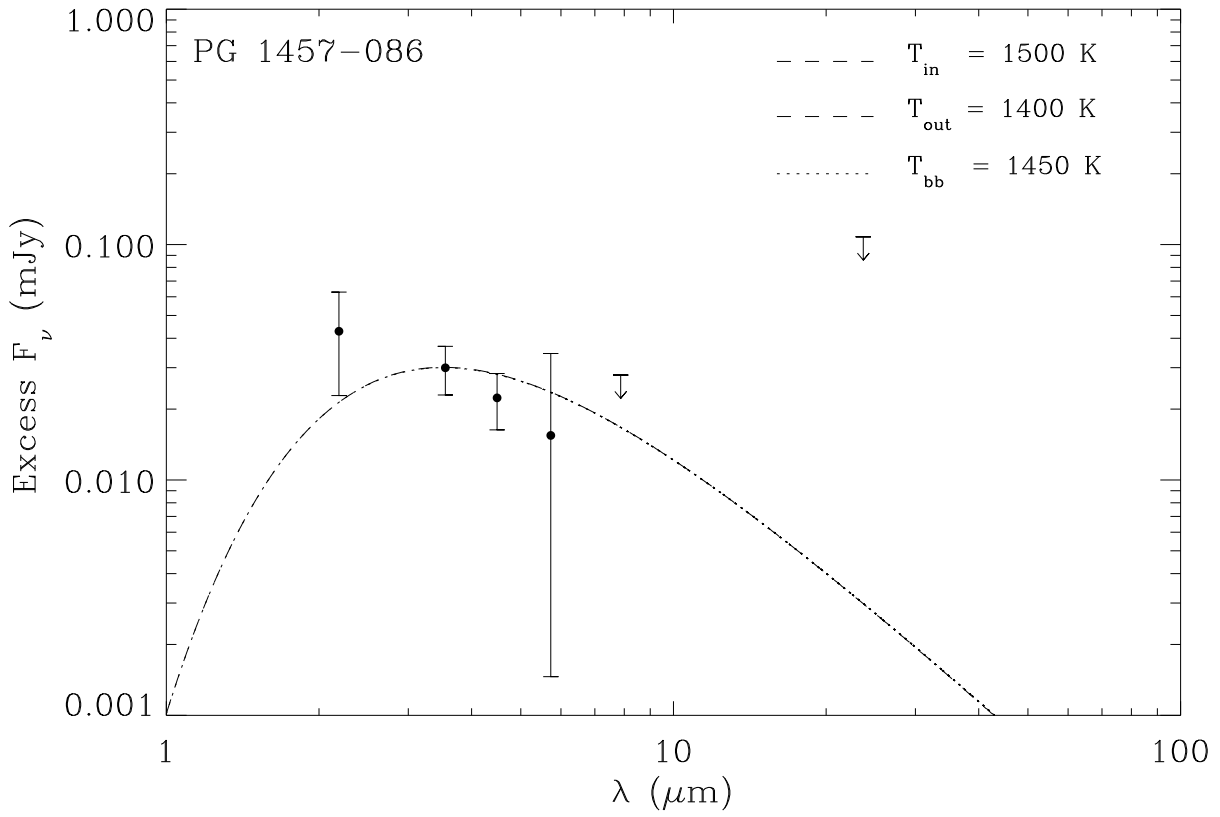
Fig. 10.— Excess infrared emission above the stellar photosphere from PG 1457−086 fitted with a model circumstellar disk with $i = 73°$ (see Figure 9 caption). The 1450 K blackbody well approximates the optically thick, narrow ring.
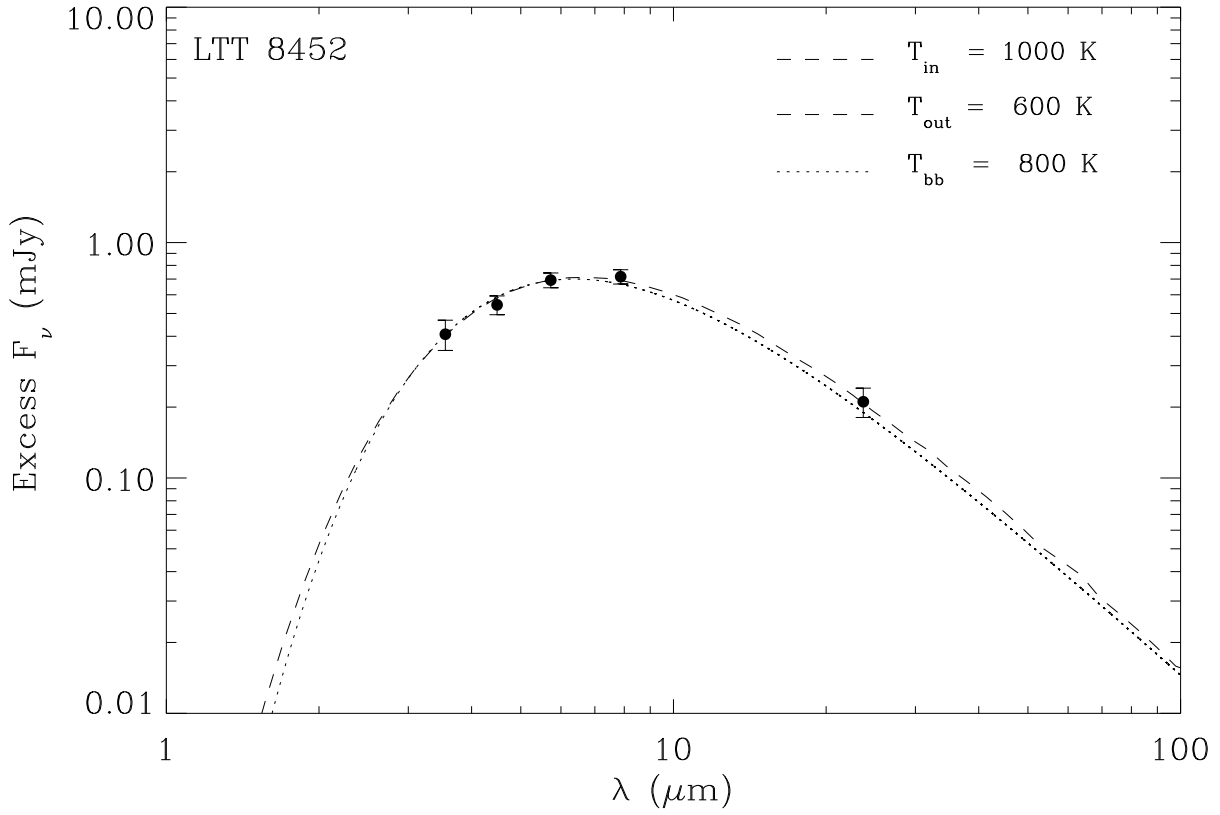
Fig. 11.— Excess infrared emission above the stellar photosphere from LTT 8452 fitted with a model circumstellar disk. The 800 K blackbody approximates the optically thick, narrow ring with a temperature range of $1000 - 600$ K.
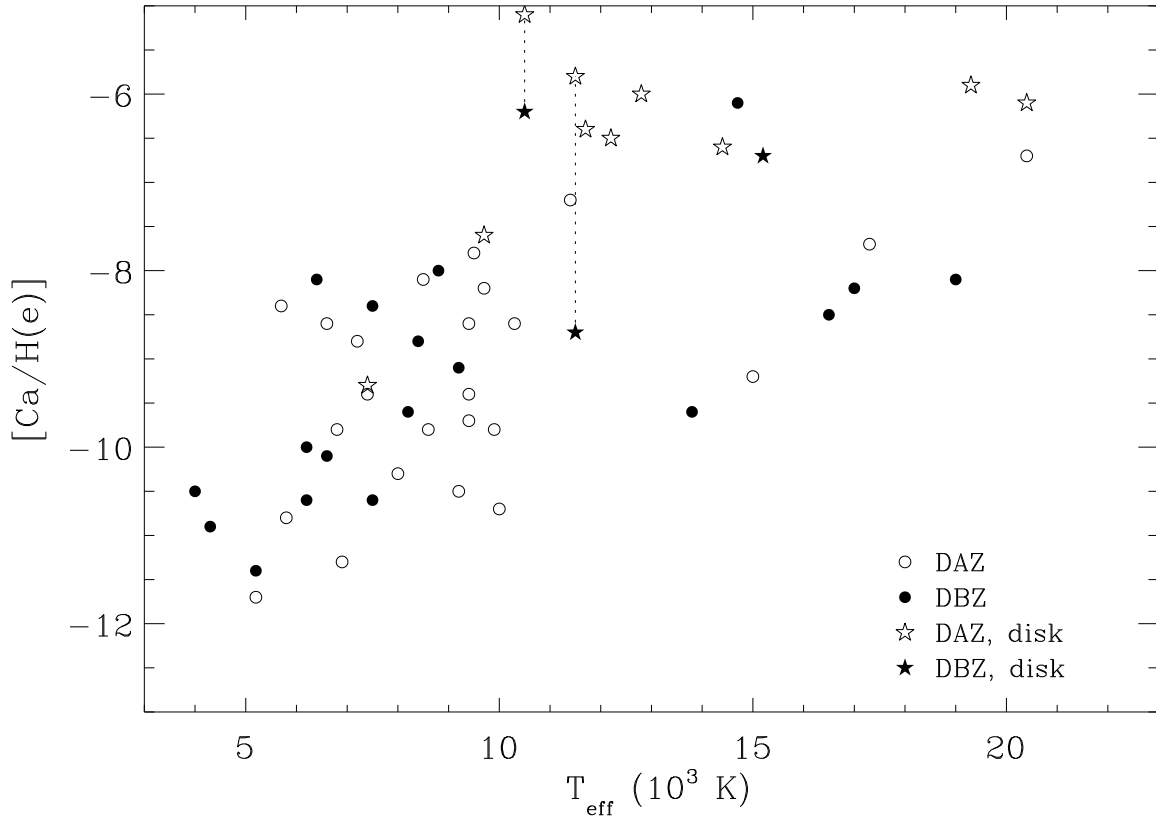
Fig. 12.— Calcium to hydrogen (for DAZ stars) and calcium to helium (for DBZ stars) abundance ratios for all metal-contaminated white dwarfs studied by *Spitzer* IRAC. In the plot, GD 16 and GD 362, both of spectral type DAZB (Table 4), are plotted both as DAZ and as DBZ stars, their data points connected by dotted lines. A typical uncertainty in the calcium abundance is 0.1 dex.
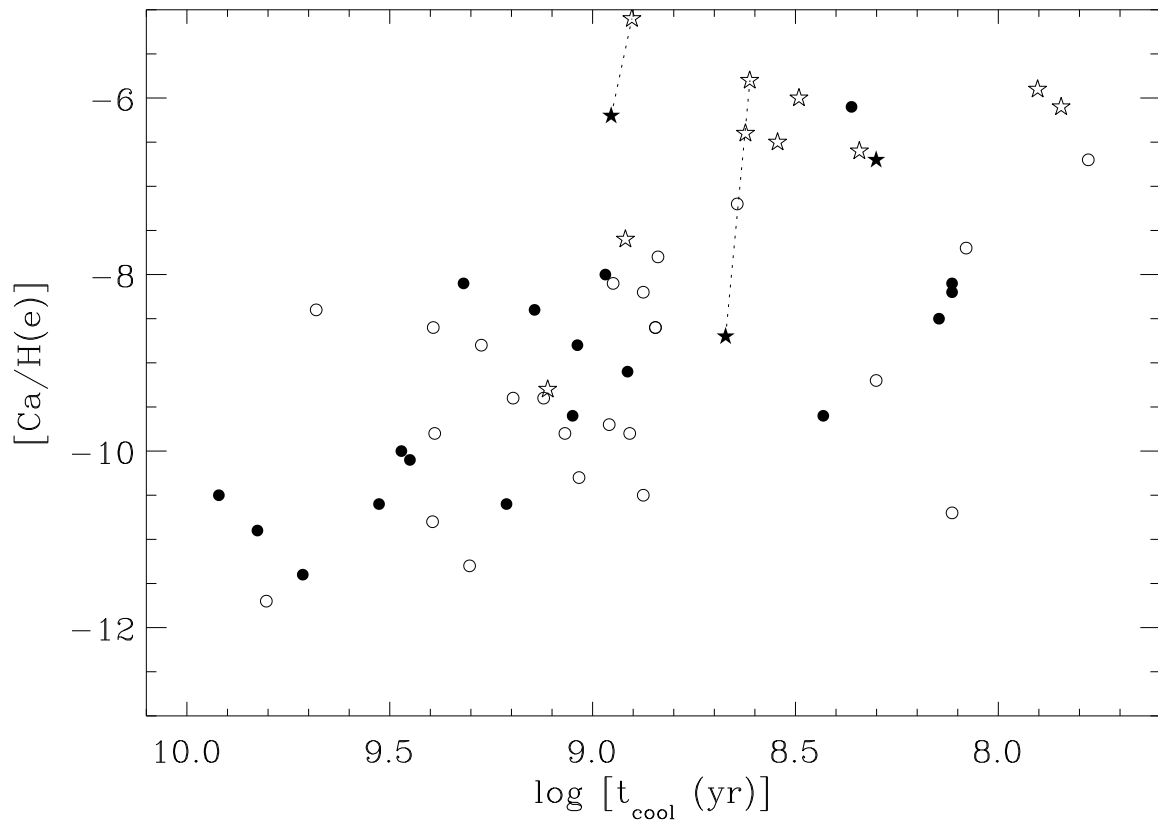
Fig. 13.— Same as Figure 12 but plotted versus cooling age.
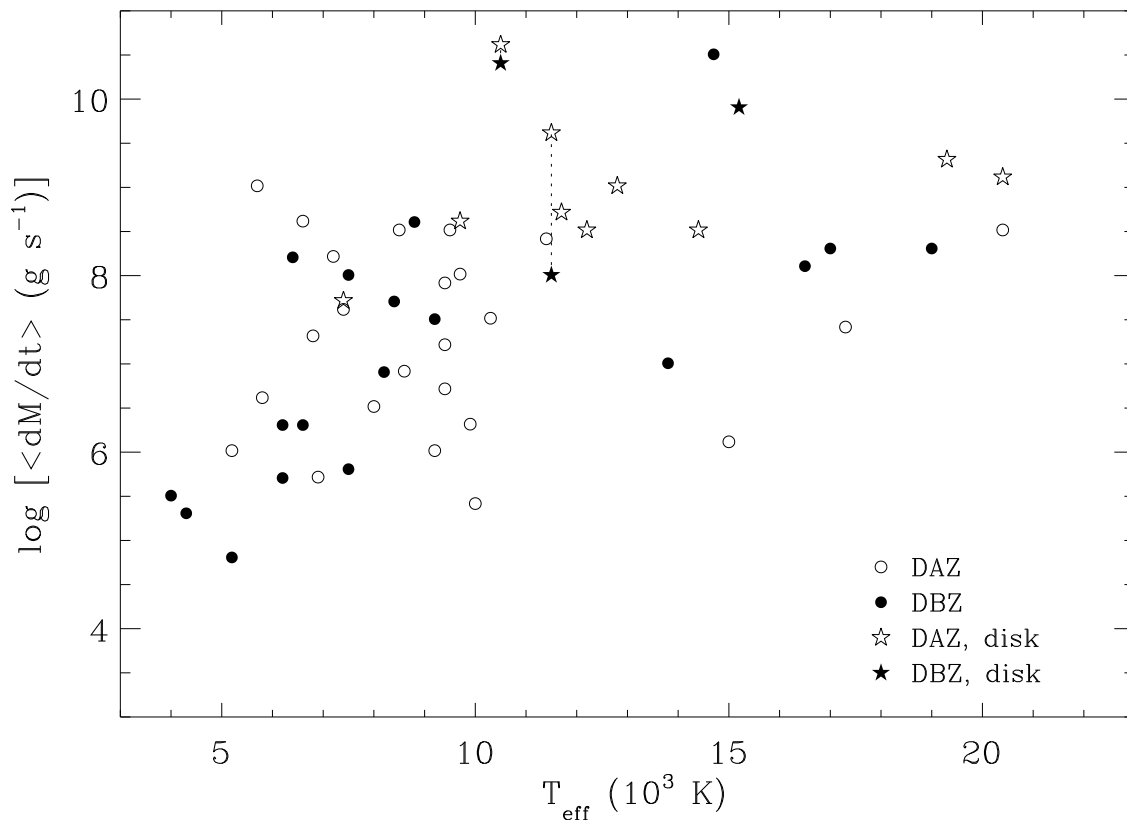
Fig. 14.— Time-averaged dust accretion rates for all metal-contaminated white dwarfs studied by *Spitzer* IRAC. Calculations were made using calcium diffusion times and convective envelope mass fractions from Koester & Wilken (2006) for DAZ stars and from Paquette et al. (1986) for DBZ stars. In the plot, GD 16 and GD 362, both of spectral type DAZB (Table 4), are plotted both as DAZ and as DBZ stars, their data points connected by dotted lines. A typical uncertainty in the accretion rate is 25%.

Fig. 15.— Same as Figure 14 but plotted versus cooling age.
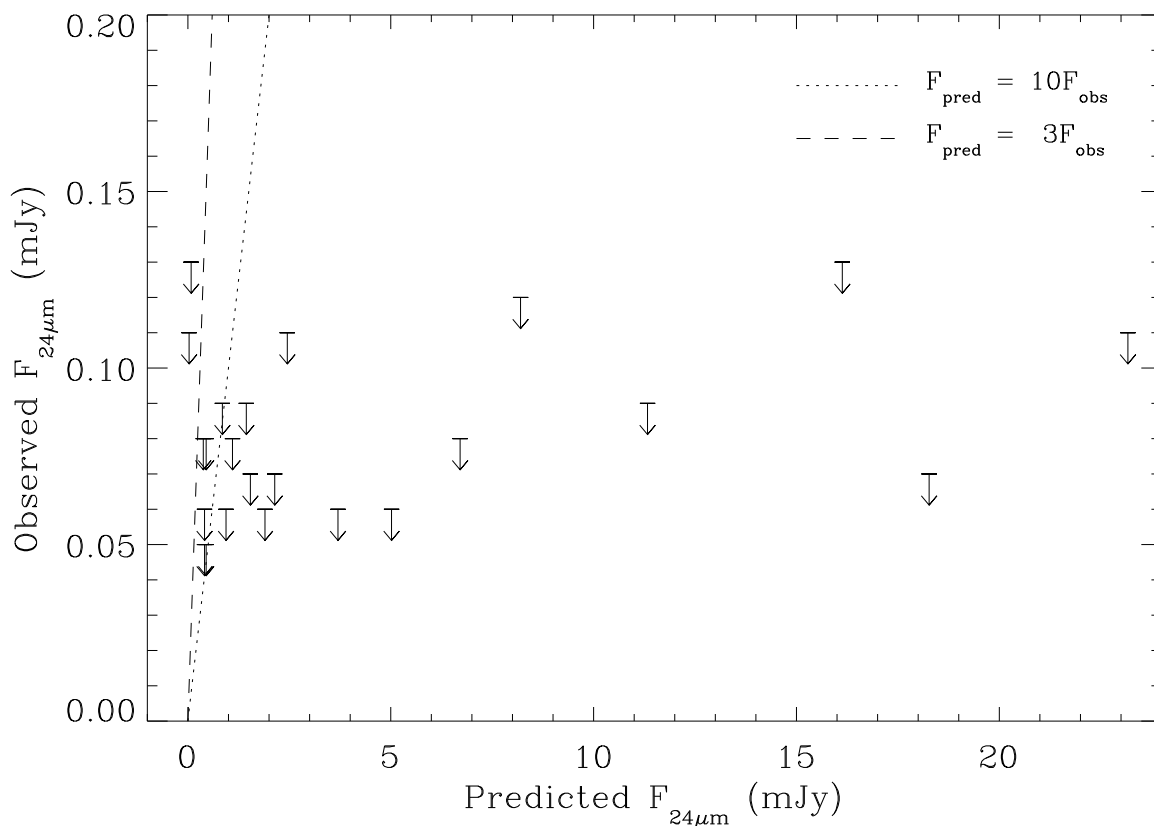
Fig. 16.— Predicted infrared fluxes at 24 μm, assuming Bondi-Hoyle accretion of interstellar matter followed by Poynting-Robertson drag, plotted versus 3σ upper limits for 25 metal-rich white dwarfs observed with MIPS at this wavelength. Stars with MIPS 24 μm detections that are consistent with warm circumstellar dust are not plotted, as well as those white dwarfs which suffered photometric contamination due to nearby sources.

Table 1.   White Dwarfs with Dust Disks

WD	Name	SpT	T_{eff} (K)	d (pc)	K (mag)	Discovery Year	Discovery Telescope	Reference
0146+187	GD 16	DAZB	11500	48	15.3	2008	*Spitzer*	1
0300−013	GD 40	DBZ	15200	74	15.8	2007	*Spitzer*	2
0408−041	GD 56	DAZ	14400	72	15.1	2006	IRTF	3
0842+231[a]	Ton 345	DBZ	18600	100	15.9	2008	CFHT/Gemini	4,5
1015+161	PG	DAZ	19300	91	16.0	2007	*Spitzer*	2
1041+092[a]	SDSS 1043	DAZ	18300	224	$\cdots$	2008	*Spitzer*	5
1116+026	GD 133	DAZ	12200	38	14.6	2007	*Spitzer*	2
1150−153	EC	DAZ	12800	76	15.8	2007	IRTF	6
1226+110[a]	SDSS 1228	DAZ	22200	142	16.4	2007	*Spitzer*	7
1455+298	G166-58	DAZ	7400	29	14.7	2008	*Spitzer*	8
1457−086	PG	DAZ	20400	110	16.0	2008	*Spitzer*	1
1729+371	GD 362	DAZB	10500	57	15.9	2005	IRTF/Gemini	9,10
2115−560	LTT 8452	DAZ	9700	22	14.0	2007	*Spitzer*	11
2326+049	G29-38	DAZ	11700	14	12.7	1987	IRTF	12

[a]These stars with circumstellar gaseous metals are not analyzed in this paper. The WD numbers for SDSS 1228, SDSS 1043, and Ton 345 are unofficial, but correctly reflect the conventional use of epoch B1950 coordinates.

References. — (1) This work; (2) Jura et al. 2007a; (3) Kilic et al. 2006; (4) Melis et al. 2008; (5) C. Brinkworth 2008, private communication; (6) Kilic & Redfield 2007; (7) Brinkworth et al. 2008; (8) Farihi et al. 2008b; (9) Becklin et al. 2005; (10) Kilic et al. 2005; (11) von Hippel et al. 2007; (12) Zuckerman & Becklin 1987b

Table 2.   Metal-Contaminated White Dwarf Targets

WD	Name	SpT	V (mag)	[Ca/H(e)][a]	References
0046+051	vMa 2	DZ	12.39	−10.0	1
0146+187[b]	GD 16	DAZB	15.5	−5.8[c]	2
				−8.7[d]	2
0208+396	G74-7	DAZ	14.51	−8.8	3
0738−172	LHS 235	DZA	13.06	−10.9	1
1202−232	EC	DAZ	12.79	−9.8	3
1257+278	G149-28	DAZ	15.41	−8.1	3
1328+307	G165-7	DZ	16.03	−8.1	1
1337+705	G238-44	DAZ	12.77	−6.7	3
1457−086	PG	DAZ	15.77	−6.1	4
1532+129[b]	G137-24	DZ	15.07	−8.4	5
1626+368	G180-57	DZA	13.85	−8.8	1
1633+433	G180-63	DAZ	14.84	−8.6	3
1653+385[b]	NLTT 43806	DAZ	15.9	−8.4	6
1705+030	G139-13	DZ	15.20	−10.1	1
1858+393	G205-52	DAZ	15.63	−7.8	3
2115−560	LTT 8452	DAZ	14.28	−7.6	4
2215+388	GD 401	DZ	16.20	−8.0	7
2251−070	LHS 69	DZ	15.71	−10.5	1
2253+803	HS	DBAZ	16.1	−6.1	8
2312−024	G157-35	DZ	16.31	−10.6	1

[a]A typical calcium abundance error is 0.1 dex.

[b]The WD numbers for G137-24, GD 16, and NLTT 43806 are unofficial, but correctly reflect the conventional use of epoch B1950 coordinates. Magnitudes with a single decimal precision are estimates and based on photographic data (e.g. McCook & Sion 2006; Monet et al. 2003).

[c][Ca/H]

[d][Ca/He]

References.   — (1) Dufour et al. 2007; (2) Koester et al. 2005b; (3) Zuckerman et al. 2003; (4) Koester et al. 2005a; (5) Kawka et al. 2004; (6) Kawka & Vennes 2006; (7) Dupuis et al. 1993; (8) Friedrich et al. 1999

Table 3.   Mid-Infrared Fluxes and Upper Limits for White Dwarf Targets

WD	$F_{3.6\mu m}$ (μJy)	$F_{4.5\mu m}$ (μJy)	$F_{5.7\mu m}$ (μJy)	$F_{7.9\mu m}$ (μJy)	$F_{24\mu m}$ (μJy)
0046+051[a]	8040 ± 400	5360 ± 270	3680 ± 190	2080 ± 110	110 ± 30
0108+277[b]	357 ± 56	226 ± 23	140 ± 19	82 ± 29	80^{c}
0146+187	486 ± 24	508 ± 25	473 ± 24	449 ± 23	120 ± 40
0208+396[a]	$\cdots$	723 ± 36	$\cdots$	268 ± 29	80^{c}
0738−172	2930 ± 150	1810 ± 90	1350 ± 100	710 ± 70	$\cdots$
1202−232[a]	$\cdots$	2010 ± 100	$\cdots$	664 ± 34	330^{c}
1257+278	290 ± 15	180 ± 9	128 ± 7	64 ± 4	70^{c}
1328+307	225 ± 11	148 ± 7	96 ± 6	52 ± 5	70^{c}
1334+039[b]	2670 ± 130	1782 ± 89	1195 ± 60	698 ± 35	70^{c}
1337+705[a]	$\cdots$	742 ± 37	$\cdots$	241 ± 14	70 ± 20
1457−086	114 ± 7	76 ± 6	49 ± 19	46^{c}	110^{c}
1532+129	413 ± 21	275 ± 14	180 ± 10	112 ± 7	60^{c}
1626+368	1033 ± 52	666 ± 33	441 ± 22	235 ± 12	60 ± 20
1633+433[a]	912 ± 46	623 ± 31	389 ± 20	232 ± 12	50^{c}
1653+385	230 ± 12	152 ± 8	93 ± 6	56 ± 5	50^{c}
1705+030	507 ± 25	339 ± 17	217 ± 12	119 ± 8	80^{c}
1858+393[a]	201 ± 10	116 ± 6	73 ± 6	54 ± 5	60^{c}
2115−560[a]	1118 ± 56	1009 ± 50	991 ± 50	876 ± 45	230 ± 30
2215+388	110 ± 6	72 ± 4	43 ± 4	23 ± 4	60^{c}
2251−070	1356 ± 68	929 ± 46	616 ± 32	406 ± 23	130^{c}
2253+803	80 ± 4	50 ± 3	35 ± 5	19 ± 3	70^{c}
2312−024	199 ± 10	133 ± 7	91 ± 6	43 ± 6	90^{c}

Note. — Error calculations, including both photometric measurements and instrumental uncertainties are described in §2.

[a]IRAC fluxes for these objects have been previously reported (Farihi et al. 2008a,b; Debes et al. 2007; Mullally et al. 2007). The photometric measurements presented here were performed independently.

[b]Not metal-polluted; see §3.6

[c]3σ upper limit.

Table 4.   Metal-Contaminated White Dwarfs Observed by *Spitzer*

WD	Name	SpT	M ($M_\odot$)	$T_{\rm eff}$ (K)	$t_{\rm cool}$ (Gyr)	[H/He]	$\log < dM/dt >$[a] (g s^{-1})	References
0002+729	GD 408	DBZ	0.59	13800	0.27	−6.0	7.0	1,2
0032−175	G266-135	DAZ	0.60	9200	0.75	⋯	6.0	3,4
0046+051	vMa 2	DZ	0.69	6200	2.96	−3.2	6.3	1,4,5
0146+187[b]	GD 16	DAZB	0.59	11500	0.47[c]	−2.9	8.0[c]	5,6
					0.41[d]		9.6[d]	
0208+396	G74-7	DAZ	0.66	7200	1.88	⋯	8.2	3,5,7
0235+064	PG	DAZ	0.61	15000	0.20	⋯	6.1	4,7
0243−026	LHS 1442	DAZ	0.70	6800	2.45	⋯	7.3	7,8
0245+541	G174-14	DAZ	0.76	5200	6.37	⋯	6.0	3,7
0300−013[b]	GD 40	DBZ	0.59	15300	0.20	−6.0	9.9	9,10
0322−019	G77-50	DZA	0.60	5200	5.18	⋯	4.8	8,11
0408−041[b]	GD 56	DAZ	0.60	14400	0.22	⋯	8.5	8,10
0552−041	G99-44	DZ	0.61	4300	6.70	−5.0[e]	5.3	2,9
0738−172	LHS 235	DZA	0.62	7600	1.63	−3.4	5.8	5,12
0843+358	GD 95	DZ	0.58	8200	1.12	−5.5[e]	6.9	2,13
0846+346	GD 96	DAZ	0.59	7400	1.32	⋯	7.6	3,4
1015+161[b]	PG	DAZ	0.61	19300	0.08	⋯	9.3	8,10
1102−183	EC	DAZ	0.60	8000	1.08	⋯	6.5	3,4
1116+026[b]	GD 133	DAZ	0.59	12200	0.35	⋯	8.5	8,10
1124−293	EC	DAZ	0.63	9700	0.75	⋯	8.0	4,8
1150−153[b]	EC	DAZ	0.60	12800	0.31	⋯	9.0	8,14
1202−232	EC	DAZ	0.66	8600	1.17	⋯	6.9	2,3
1204−136	EC	DAZ	0.61	11400	0.44	⋯	8.4	4,8
1208+576	G197-47	DAZ	0.56	5800	2.48	⋯	6.6	3,4
1225+006	HE	DAZ	0.66	9400	0.91	⋯	6.7	8,10
1257+278	G149-28	DAZ	0.58	8500	0.89	⋯	8.5	3,5,7
1315−110	HE	DAZ	0.86	9400	1.57	⋯	7.2	8,10
1328+307	G165-7	DZ	0.57	6400	2.08	−3.0	8.2	5,12
1337+705	G238-44	DAZ	0.58	20400	0.06	⋯	8.5	2,3,5
1344+106	G63-54	DAZ	0.65	6900	2.01	⋯	5.7	3,4
1407+425	PG	DAZ	0.67	9900	0.81	⋯	6.3	3,4
1455+298[b]	G166-58	DAZ	0.58	7400	1.29	⋯	7.7	3,4
1457−086[b]	PG	DAZ	0.62	20400	0.07	⋯	9.1	5,8,10
1532+129	G137-24	DZ	0.58	7500	1.39	⋯	8.0	5,15
1626+368	G180-57	DZA	0.59	8400	1.09	−3.6	7.7	5,12
1632+177	PG	DAZ	0.58	10000	0.13	⋯	5.4	3,4

Table 4—Continued

WD	Name	SpT	M $(M_\odot)$	$T_{\rm eff}$ (K)	$t_{\rm cool}$ (Gyr)	[H/He]	$\log < dM/dt >$[a] (g s^{-1})	References
1633+433	G180-63	DAZ	0.68	6600	2.47	$\cdots$	8.6	3,4,5
1653+385	NLTT 43806	DAZ	0.77	5700	4.80	$\cdots$	9.0	5,16
1705+030	G139-13	DZ	0.70	6600	2.82	-3.6	6.3	5,12
1729+371[b]	GD 362	DAZB	0.73	10500	0.90[c]	-1.1	10.4[c]	17,18
					0.80[d]		10.6[d]	
1822+410	GD 378	DBAZ	0.55	17000	0.13	-4.0	8.3	1,2
1826$-$045	G21-16	DAZ	0.73	9400	0.70	$\cdots$	7.9	4,8
1858+393	G205-52	DAZ	0.59	9500	0.69	$\cdots$	8.5	3,4,5
2105$-$820	LTT 8381	DAZ	0.60	10300	0.70	$\cdots$	7.5	2,8
2115$-$560[b]	LTT 8452	DAZ	0.66	9700	0.83	$\cdots$	8.6	2,5,8
2144$-$079	G26-31	DBZ	0.55	16500	0.14	$\cdots$	8.1	8,10
2149+021	G93-48	DAZ	0.59	17300	0.12	$\cdots$	7.4	2,8
2215+388	GD 401	DZ	0.58	8800	0.93	-3.4[e]	8.6	5,13
2216$-$657	LTT 8962	DZ	0.58	9200	0.82	-4.0	7.5	1,2
2251$-$070	LHS 69	DZ	0.58	4000	8.34	-6.0[e]	5.5	5,12
2253+803	HS	DBAZ	0.59	14700	0.23	-5.5	10.5	1,5
2312$-$024	G157-35	DZ	0.69	6200	3.36	-4.9	5.7	5,12
2326+049[b]	G29-38	DAZ	0.62	11700	0.42	$\cdots$	8.7	8,4,19
2354+159	PG	DBZ	0.55	19000	0.13	$\cdots$	8.3	8,10

[a]A typical error in the calculated accretion rate is 25%, arising from a typical 0.1 dex error in the measured calcium abundance.

[b]Circumstellar disk detected.

[c]Calculated for a DBZ white dwarf.

[d]Calculated for a DAZ white dwarf.

[e]Upper limit.

References. — (1) Wolff et al. 2002; (2) Mullally et al. 2007; (3) Zuckerman et al. 2003; (4) Farihi et al. 2008a; (5) This work; (6) Koester et al. 2005b; (7) Debes et al. 2007; (8) Koester et al. 2005a; (9) Voss et al. 2007; (10) Jura et al. 2007a; (11) Farihi et al. 2008b; (12) Dufour et al. 2007; (13) Dupuis et al. 1993; (14) Jura et al. 2009; (15) Kawka et al. 2004; (16) Kawka & Vennes 2006; (17) Zuckerman et al. 2007; (18) Jura et al. 2007b; (19) Reach et al. 2005

Table 5.   Carbon-Poor and Metal-Rich White Dwarfs

WD	Name	[C/Fe][a]	Dust?	Reference
0002+729	GD 408	−0.6	N	1
0100−068	G270-124	−0.6	N	1
0300−013	GD 40	−1.0	Y	2
0435+410	GD 61	−1.2[b]	⋯	⋯
1626+368	G180-57	−0.7[b]	N	3
1729+371	GD 362	0.0[b]	Y	4
2253+803	HS	−2.4[b]	N	3

[a]Iron and carbon abundances and upper limits taken from Desharnais et al. (2008); Zuckerman et al. (2007); Wolff et al. (2002); a typical error in this ratio is 0.3 dex.

[b]Upper limit.

References. — (1) Mullally et al. 2007; (2) Jura et al. 2007a; (3) This work; (4) Jura et al. 2007b

Table 6.   Target Ages and Upper Mass Limits for Unresolved IRAC Companions

WD	$t_{\rm ms}$ (Gyr)	$t_{\rm cool}$ (Gyr)	$t_{\rm total}$ (Gyr)	d (pc)	$M_{4.5}$ (mag)	Mass ($M_{\rm J}$)
0002+729	1.9	0.3	2.2	35	14.0	18
0108+277[a]	0.2	7.0	7.2	14	15.3	20
0552−041	1.2	6.7	7.9	6.5	15.4	18
0738−172	1.1	1.6	2.7	8.9	14.8	13
0843+358	2.5	1.1	3.6	24	14.7	17
1202−232	0.6	0.9	1.5	11	14.2	12
1225+006	0.6	0.9	1.5	30	14.5	11
1315−110	0.1	1.5	1.6	33	14.7	11
1328+307	3.2	2.1	5.3	30	14.9	18
1334+039[a]	6.3	4.9	11.2	8.2	15.0	25
1337+705	2.5	0.1	2.6	25	13.5	25
1532+129	2.5	1.4	3.9	23	14.8	17
1626+368	1.9	1.0	2.9	16	14.6	15
1653+385	0.2	4.9	5.1	15	16.3	10
1705+030	0.4	2.7	3.1	18	15.1	12
1822+410	6.3	0.1	6.4	50	13.3	40
2105−820	0.6	0.7	1.3	18	14.3	11
2149+021	1.9	0.1	2.0	25	13.5	20
2144−079	6.3	0.1	6.4	69	13.3	40
2215+388	2.5	0.9	3.4	51	14.4	18
2216−657	2.5	0.8	3.3	24	14.6	17
2251−070	2.5	8.3	10.7	8.1	15.7	20
2253+803	1.9	0.2	2.1	85	13.6	20
2312−024	0.4	3.4	3.8	27	15.2	13
2354+159	6.3	0.1	6.4	105	13.5	40

[a]Not metal-polluted; see §3.6

Note. — Stellar parameters are taken from the literature (see Table 2 references). For stars with no mass or surface gravity determination, $\log g = 8.0$ was assumed.

Table 7. Target Ages and Upper Mass Limits for Resolved IRAC Companions

WD	t_{ms} (Gyr)	t_{cool} (Gyr)	t_{total} (Gyr)	d (pc)	$M_{7.9}$ (mag)	Mass (M_{J})
0108+277[a]	0.2	7.0	7.2	14	14.3	60
0738−172	1.1	1.6	2.7	8.9	14.0	50
1334+039[a]	6.3	4.9	11.2	8.2	15.4	50
1532+129	2.5	1.4	3.9	23	13.2	70
1626+368	1.9	1.0	2.9	16	14.0	50
1653+385	0.2	4.9	5.1	15	14.1	60
1705+030	0.4	2.7	3.1	18	13.7	60
2251−070	2.5	8.3	10.7	8.1	14.7	60

[a]Not metal-polluted; see §3.6

Note. — The exposure time for 0738−172 was only 60 s versus 600 s for the primary six targets, resulting in an overall sensitivity about 1/3 that calculated in Farihi et al. (2008b), while for 2251−070 the total integration time was 150 s and hence this target had an overall sensitivity about 1/2 that of the primary target stars.